

Estimation of Disturbance and Energy Consumption
for Quadruped Robot Control

(4足ロボット制御のための外乱および
消費エネルギーの推定)

January, 2019

Doctor of Philosophy (Engineering)

Ryosuke Horio

堀尾 亮介

Toyohashi University of Technology

Contents

Chapter 1	Introduction	1
1.1	Background	1
1.2	Review on the Field of Walking Robot	3
1.3	Objectives and Methods	6
1.4	Thesis Organization	7
Chapter 2	Preliminaries of Legged-Locomotion	9
2.1	Gaits	9
2.2	Parameters for Legged-Locomotion	10
2.3	Cost of Transportation	11
2.4	Zero-Moment Point and Table-Cart Model	13
Chapter 3	Review on Conventional Studies	15
3.1	Motion Control of Quadruped Robot Based on Inclination of Body .	15
3.1.1	Robot Model and Motion Trajectory	16
3.1.2	Controller Design based on Inclination of body	20
3.1.3	Simulation Conditions and Results	24
3.2	Energy Consumption for Locomotion	28
3.3	Central Pattern Generator	32
Chapter 4	Estimation of Energy Consumption	35
4.1	Introduction	35
4.2	Simulation of Energy Consumption	35
4.2.1	Dynamics Model	35
4.2.2	Simulation Conditions	36
4.2.3	Simulation Results	38
4.3	Experimental Validation of Proposed Model	40
4.3.1	Robot Design and Experimental Conditions	40

	4.3.2	Experimental Results	41
	4.3.3	Discussion	42
Chapter 5		Estimation of Disturbance and Ground Reaction Force	43
5.1		Disturbance Observer for Estimating Disturbance Force of a Biped Robot	43
	5.1.1	Introduction	43
	5.1.2	Dynamics Model	46
	5.1.3	Observer Design	47
	5.1.4	Simulation Conditions	49
	5.1.5	Simulation Results	52
	5.1.6	Discussion	53
5.2		Disturbance Observer for Estimating Ground Reaction Force of a Quadruped Robot	56
	5.2.1	Introduction	56
	5.2.2	Dynamics Model	56
	5.2.3	Estimation of Ground Reaction Force	57
	5.2.4	Simulation Conditions	59
	5.2.5	Simulation Results	64
	5.2.6	Discussion	64
Chapter 6		Conclusion	67
6.1		Summary	67
6.2		Discussion	68
		Bibliography	71
		Acknowledgment	80

Chapter 1

Introduction

1.1 Background

In recent years, large-scale disasters such as the Tohoku Earthquake in 2011 are occurring frequently. As the result of the Earthquake, in the accident of the Fukushima Daiichi Nuclear Power Plant, workers working in the vicinity of the reactor building were damaged from the poor environment [1].

Meanwhile, countermeasures against a declining birthrate and an aging society are urgent in Japan, but the number of people engaged in nursing care for elderly is insufficient and the load on caregivers has also increased [2]. Also in the construction industry, skill workers are aging, and shortage of workers is getting worse. Currently there are about 3.3 million workers in the construction industry, but there are views that the number of the workers will fall to 2.16 million in 2025 [3]. In the field of transportation, decreasing number of workers is concerned as well [4].

In view of the above circumstances, introducing robots that perform dangerous work or hard labor on behalf of human is desired [5]. For example, in a dangerous place where human can not enter, necessity of robots to act on behalf of human is considered. In fact, robots are introduced in work that deal with substances harmful to the human body, such as painting processes at automobile factories etc. [6]. Robots were also utilized for surveying inside the reactor building of Fukushima Daiichi Nuclear Power Station [7]. Introducing nursing care robots is also being considered in the field of nursing care, and demand for robots that can effectively provide nursing care are increasing [8].

In general, most industrial robots used in factories do not need to move, and transport robots that carry out moving operations need to travel only on a flat floor or rails. However, robots working outdoors such as in disaster or construction sites with obstacles, steps and uneven terrain are required to have the following abilities:

- Adjusting to unknown conditions such as rough terrain and steps, and avoiding obstacles
- Avoiding stumbling or maintaining the standing state
- Being robust to dirt and moisture environment

In addition, it is not reasonable for a mobile robot to work with tethering cables which supply power from energy source out of the robot. Thus energy of the robot working outdoors is usually covered by built-in batteries or generators and this causes limitation of operating time.

As mentioned above, the robots operated outdoors are required to handle unknown terrain conditions and stand-alone activities. Walking robots, which are the robots walk with their legs are one of the solutions for practical implementation of the mobile robots. Their advantages over mobile robots with wheels or crawlers lie in their structural feature; having legs. The legs allow them to adapt to various environments such as disaster or construction sites with obstacles, steps and uneven terrain (Fig. 1.1). Even in entertainment use, they are possibly expected to walk up stairs.

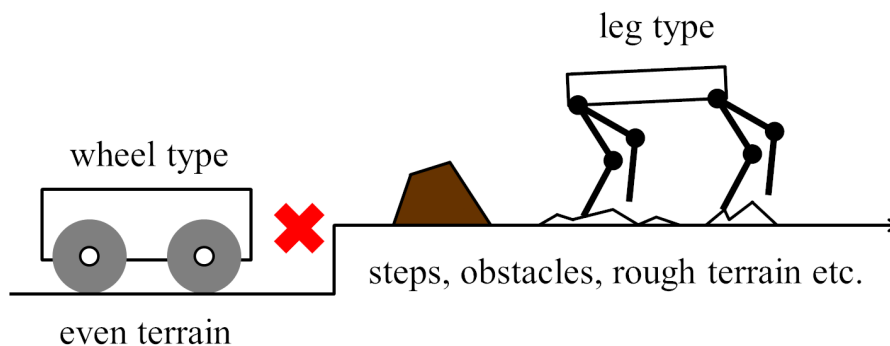


Fig. 1.1 Comparison of mobility capability

Furthermore, it is thought that stable locomotion is easier to be achieved with a multi-legged robot (generally four legs or more) on rough terrain compared with a biped robot. This is because a robot with four or more legs is very stable to stand in a stationary state and can support its body with three or more legs depending on the situation even while locomotion. In addition, quadruped locomotion is said to be able to combine maneuverability and walking ability in multi-legged walking. This is because the robot's weight increases and the leg control becomes difficult, such as narrowing the range of motion of the legs, as the number of legs increases. Thus, the quadruped locomotion has

many characteristics suitable for activities in rough terrain, it is thought that it has high versatility for various topographies, and it is expected to be used in rough terrain.

Although the present practical walking robots are mostly for entertainment-use, such as Aibo [9] and ASHIMO [10], they are getting more attention in several commercial fields such as construction [11]. SpotMini (Fig. 1.2) is a quadruped robot developed by Boston Dynamics. It has been examined in demonstration experiments conducted by Takenaka Corporation, SoftBank Robotics Corp. and SoftBank Corp. on construction sites for practical application in 2019. [3, 12] and scheduled for large-scale production for general sale from middle of 2019 [13].



Fig. 1.2 SpotMini developed by Boston Dynamics [11]. It weighs 25 kg (30 kg including the 5 degree-of-freedom arm) and driven by batteries lasting for 90-minute operation time on a charge. It has perception sensors including stereo cameras, depth cameras, an inertia measurement unit, and position/force sensors in the limbs.

1.2 Review on the Field of Walking Robot

Considering those prospectives that the walking robots will be used in various fields as mentioned above, numerous studies on walking robots have been conducted. There are various approaches to achieve fast, stable and energy-efficient locomotion for developing a practical walking robot.

Model-based controller design is one of those approaches to locomotion control. In the model-based approach, dynamics of the robot is derived to design the locomotion controller. In general, it is inconvenient to utilize the complete dynamics of the robot due

to its complexity, thus an approximated model is considered by ignoring some mechanical components and nonlinearity.

The model-based approach is useful to analyze and understand the behavior of the robot system. One of the simplest models is the table-cart model that considers simple dynamics of a cart with concentrated mass moving on a table, that corresponds to the robot's center of gravity. This model includes an important index for stable locomotion of walking robots known as Zero-Moment Point (ZMP), which can be calculated by measuring ground reaction force acting on legs [14, 15]. It is often considered as an index for stable locomotion designing a motion controller [16–22]. Similarly, based on the strategy of stable locomotion suggested by the idea of the ZMP, a sprawling-type robot with a large supporting leg polygon and low center of gravity is proposed [23]. Besides the ZMP, there are several attempts of the motion control of walking robots. The author considered posture of robot's body as an index for stable locomotion and proposed a controller design based on inclination of its body [24]. Focchi et al. focused on torque controller design to achieve quasi-static locomotion on a steep slope, which requires regulation of ground reaction force [25]. Zhang et al. considered full dynamics of a quadruped robot running in trotting for stable torso motion [26]. The ground reaction force including leg tip impact and friction is often taken into account in the model-based approach such as biped locomotion dynamics based on the energetic approach considering energy of propulsion provided by the rear leg and energy lost during the impact of the front leg [27], a biped robot dynamics model with nonlinear friction of the floor [28] and a leg mechanism for a regenerative shock absorber [29].

On the other hand, there are many attempts to apply locomotive mechanisms of walking animals to robots rather than considering controller design based on their dynamics. Quadruped animals have developed their locomotive abilities and body structures to adapt to various terrain. Applying locomotive mechanisms of animals to robots may enable them to achieve stable, fast and energy-efficient locomotion. Bio-inspired studies mainly focus on unraveling animals' automatic locomotion regulation mechanism. Rosendo et al. developed a cheetah-like robot which has musculoskeletal structure inspired by cheetahs to replicate rhythmical muscular activation based on stretch and reflex of artificial muscles [30,31]. Mutlu and Hauser et al. considered compliant joints and foot mechanism for locomotion on rough terrain [32,33]. Combination of bio-inspired structure of robots and model-based approach is also considered to understand the animals' locomotion mechanism [34–38].

Generation of animals' rhythmical motion is an important research field of walking robots and numerous studies have been conducted [39–51]. Spröwitz et al. designed an experimental quadruped robot with a flexible leg structure and local phase oscillators interacting to each other inspired by the animals' neural network for regulating phase differences between legs [45]. The designed robot achieved fast locomotion with short flight phase. Those phase oscillators are known as Central Pattern Generator (CPG). Fukuoka et al. proposed CPG modulated by leg load observed in the animals' locomotion [43].

Besides the motion control, energy consumption for locomotion is also considered as it is required to reduce energy consumption for the robots' motion, especially locomotion which is the most fundamental motion of mobile robots including walking robots to extend the operating time. In studies of energy consumption for locomotion, both of the model-based and bio-inspired approaches are adopted. Seok et al. proposed a hardware design for minimization of major energy losses by employment of high torque density motors, low impedance transmission, energy regenerative electronics and a design architecture that minimizes the leg inertia [52, 53]. Krishna et al. investigated the energy consumption in a bounce gait [54]. Gao et al. proposed a controller design for reduction of energy consumption of a hexapod robot by minimizing impact force [55].

In the biological field, there are many studies on animals' locomotion [56–59]. According to the achievements of those studies, it is reported that the gait transition observed in animals who walk with their legs seems to optimize the energy required for the locomotion [56]. Thus the animals' locomotion is considered as a reference to reduce energy consumption for locomotion in robotic fields [60–63]. Kiguchi et al. applied genetic algorithm to obtain the energy-optimal gait for quadruped locomotion [63]. Nishii introduced an analytical model for estimating energy consumption of animals' locomotion, which consists of simple one leg link [60]. Nishii suggested that the distribution of the ground reaction force determines optimal duty ratio. Owaki et al. proposed a simple algorithm based on the CPG which contains phase oscillators modulated by magnitude of ground reaction force in each leg as well [40, 41]. The proposed CPG successfully produced spontaneous gait transitions depending on the robot's locomotion velocity and it was shown that the gait transition optimized energy consumption for locomotion. In those cases of the bio-inspired studies, the ground reaction force is an essential factor to understand the mechanism of animals' locomotion.

1.3 Objectives and Methods

For the practical use of quadruped robots, effective methods for reducing energy consumption of locomotion must be considered. As mentioned above, Nishii proposed a simple mathematical model for estimation of energy consumption for locomotion [60]. However, the model proposed in his study is one-link model, which is different from actual animals' or robots' legs. He also proposed a mathematical model for estimating energy consumption for locomotion of an insect [61], but the model considers full dynamics of an insect's whole body, thus it is complex and difficult to be applied to other body structures such as mammals or quadruped robots.

On the other hand, ground reaction force plays an important role for controlling a walking robot. However, measuring the ground reaction force using sensors such as a load cell restricts the leg structure. The ground reaction force is also useful to analyze the behavior of the robot, and hence its detection without sensors is favorable. Camurri showed a method to detect the contacts of leg tips based on probability of reliable contact utilizing leg odometry and internal force sensing [64]. However, his method is unable to estimate the magnitude of ground reaction force.

A disturbance observer is a possible solution to this issue. The disturbance observer is to estimate the disturbance applied to the system by comparing outputs of an actual system with ones of its nominal model. Employing the disturbance observer for the estimation of the ground reaction force enables a controller design utilizing it. However, deriving the nominal model of the robot's dynamics is generally difficult.

Considering the above-mentioned discussion, this study aims to achieve the following two objectives:

1. Propose a simple dynamics model for estimation of energy consumption for locomotion, which contributes to reducing the energy consumption of walking robots
2. Design a disturbance observer for estimation of ground reaction force, which can be applied to various controller designs such as CPG, ZMP and suppression of the energy consumption

For the first objective, a novel simple dynamics considering two legs composed of two links named "2-link 2-leg model" is proposed in this study. The model is designed to focus on the pitch motion of the robot in the sagittal plane and the motion of the fore and hind legs are treated separately to reduce the complexity of the robot's dynamics. Moreover,

the model can be extended to other body structures such as a hexapod robot by considering additional disturbance applied to the robot's body.

To achieve the second objective, an observer for estimating the ground reaction force acting on a walking robot based on the proposed model is designed. The observer is based on the high-gain observer structure and a nominal model of the observer is derived utilizing the model proposed for the estimation of the energy consumption.

The proposed model for those two objectives are verified by experiments and simulations. The energy consumption computed by utilizing the proposed model is examined by experiments on an actual robot and the obtained profile of the energy consumption is compared with the Nishii's conventional study [60]. The performance of the observer employing the proposed model is validated by simulations on Open Dynamics Engine [65].

1.4 Thesis Organization

This thesis is composed of the following chapters: In chapter 2, preliminaries of legged-locomotion are explained. In chapter 3, conventional studies which relate to this study are introduced and explained. In chapter 4, a dynamics model for estimating energy consumption for locomotion is proposed. In chapter 5, an observer design adopting the proposed model for estimating disturbance and ground reaction force acting on a walking robot is described. In chapter 6, the study achievements are summarized and the problems and future prospective are discussed.

Chapter 2

Preliminaries of Legged-Locomotion

2.1 Gaits

In this section, gaits of quadruped locomotion are explained. Quadruped locomotion is classified into several kinds of locomotion, which is called gaits, according to the order in which the legs are extended. Typical gaits are classified into the following four types [66]:

- crawl** Move one leg in the order of left fore, right rear, right fore and left rear. Since it always supports the body with three legs, it is excellent in stability. It is observed in animals walking at low speed (Fig. 2.1(a)).
- trot** Move diagonal legs (a pair of left fore and right rear legs, and pair of right fore and left rear legs) simultaneously. Because diagonal legs are raised at the same time, trot gait is harder to fall than pace, bounce described later, and has advantage on stability over them. Many of the animals with four legs walk by trot (Fig. 2.1(b)).
- pace** Move fore and rear legs (a pair of left fore and left rear legs, and pair of right fore and right rear legs) simultaneously. Pace is faster gait than trot (Fig. 2.1(c)).
- bounce** Move left and right legs (a pair of left fore and right fore legs, and pair of left rear and right rear legs) simultaneously. Among the typical gaits, bounce is most suitable gait for fast locomotion such as running (Fig. 2.1(d)).

The gaits mentioned above are typically observed in animals' locomotion, however, the gaits are classified into more detailed types according to the locomotion parameters such as phase differences among legs and duty ratio.

In the case of the trot gait, the risk of falling is lower than that of the pace gait and the bounce gait because the legs on the diagonal are moved at the same time. The locomotion at higher velocity than the crawl gait can be expected as well. On the other hand, the crawl gait locomotion can be adopted when walking on rough terrain because three or more legs always support the body.

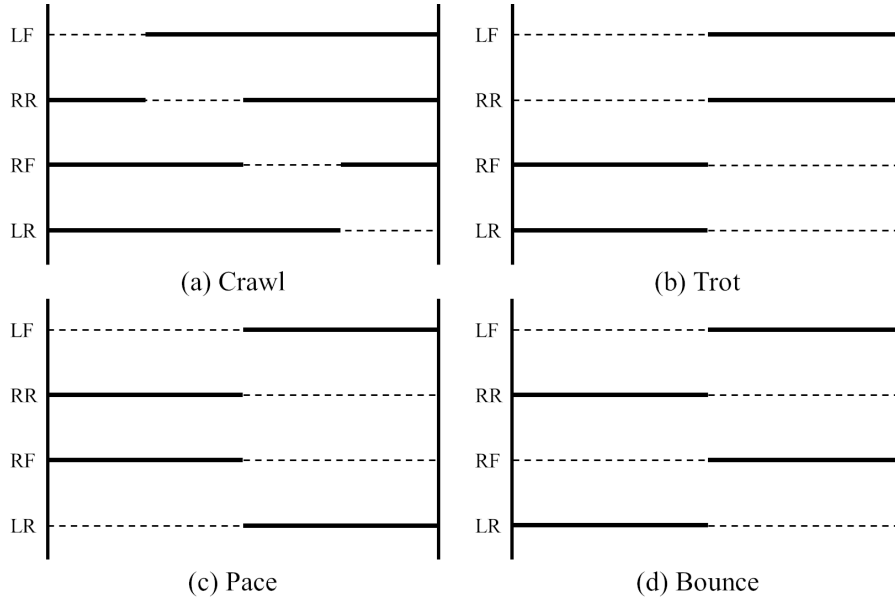


Fig. 2.1 Typical gaits. The abbreviation LF, RR, RF and LR denote left-fore, right-rear, right-fore and left-rear legs, respectively. The stance phase and swing phase are expressed by the solid and dotted lines, respectively.

2.2 Parameters for Legged-Locomotion

The gaits described in the previous section represent the order of moving the legs. Other than the gaits, the parameters representing the locomotion include the following (Fig. 2.2) .

- locomotion velocity v : velocity of the locomotion of the robot in direction of travel
- stance length s : Distance in which the robot travels during a stance phase, i.e., length of one step
- locomotion period T : Time taken for one cycle of the locomotion
- duty ratio β : Ratio of time for a stance phase to a locomotion period
- phase differences ϕ : Difference of phase among each leg

The locomotion velocity, stance length, duty ratio and locomotion period is constrained by the following equation:

$$v = \frac{s}{\beta T} \quad (2.1)$$

In Eq. 2.1, three of those parameters can be set arbitrarily. The locomotion velocity v is often set to the desired value, therefore the equation of the locomotion parameters has two-degree of freedom.

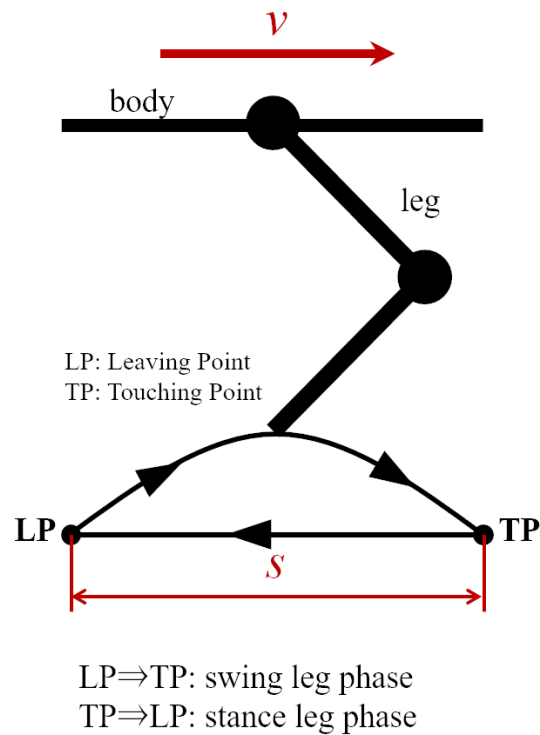


Fig. 2.2 Parameters for legged-locomotion

2.3 Cost of Transportation

In this study, the energy consumption is evaluated by cost of transportation (COT) that is dimensionless number describing energy consumed to transport a unit weight for a unit distance, namely,

$$COT[-] = \frac{e[\text{J}]}{mg[\text{N}] \cdot d[\text{m}]} \quad (2.2)$$

where e is consumed energy, m is a mass of a transported object, g is gravitational acceleration and d is distance of the transportation.

In this study, the energy consumption for locomotion is assumed to be composed of two

factors; mechanical work for motion of legs and heat loss due to generating force/torque according to Nishii's study [60]. Mechanical work done by actuators for leg motion e_m is defined as follows;

$$e_m = \int \langle \boldsymbol{\tau}, \boldsymbol{\Omega} \rangle dt \quad (2.3)$$

where $\boldsymbol{\tau}$ is an input force/torque vector and $\boldsymbol{\Omega}$ is an velocity/angular velocity vector. $\langle \rangle$ indicates an operator for inner product of two vectors. In this study, energy regeneration in actuators is ignored as it is difficult to utilize the regenerated energy in walking robots. Therefore, negative value in Eq. (2.3) is ignored:

$$e_m = \int \max(\langle \boldsymbol{\tau}, \boldsymbol{\Omega} \rangle, 0) dt \quad (2.4)$$

It is expected that mechanical work increases as locomotion velocity increases, because the joint angular velocity generally depends on locomotion velocity. Heat loss e_h due to generating force/torque is defined as follows:

$$e_h = \int c \langle \boldsymbol{\tau}, \boldsymbol{\tau} \rangle dt \quad (2.5)$$

where c is a constant coefficient. This heat loss model corresponds to the Joule heat in electrical actuators. As Eq. (2.5) does not depend on the angular velocity, but only on the input torque, the robot consumes energy for standing without any motion. Thus, it is expected that the heat loss increases as duration of stance phase, i.e., locomotion velocity decreases and duty ratio increases.

2.4 Zero-Moment Point and Table-Cart Model

In this section, Zero-Moment Point (ZMP) used as an index of conventional stable locomotion is explained. In the following, ZMP in a two-dimensional table-cart model is derived [14].

Consider a cart that moves freely on a table as shown in Fig. 2.3. It is assumed that the mass of the table is negligible and the cart is regarded as a concentrated mass. Here, the mass of the cart m , foot of the table and height from the ground to the cart z_c corresponds to the mass, supporting polygon, height to the center of gravity of the robot, respectively. The movement of the cart corresponds to the movement of the center of gravity of the robot. Take the absolute coordinate system with the origin O at the appropriate position on the ground, the x axis to the right from O , and the z axis upward vertically. The projection point p on the ground of the resultant force f is obtained by the following equilibrium equation of the moment;

$$mg(p - x) = -m\ddot{x}z_c \quad (2.6)$$

$$p = x - \frac{\ddot{x}}{g}z_c \quad (2.7)$$

where g is the gravitational acceleration and p is called the resulted ZMP. If this resulted ZMP lies inside the table's foot (the supporting polygon of the robot), the point p_r at which the ground reaction force acts coincides with the point p (Fig. 2.4 (a)). However, when the resulted ZMP is outside the foot, the ground reaction force acts on the edge of the table's feet, and a moment which tries to overturn the table by the resultant force f works (Fig. 2.4 (b)). At this time, the actual ZMP is at the center of the rotary motion the table is about to tip over and does not match the point p which is the resulted ZMP.

As mentioned above, ZMP has been used as an indicator of stable locomotion [16–22] because the stability of locomotion can be confirmed by considering whether ZMP is in supporting polygon or not. However, even if ZMP is not in the supporting polygon, swing legs can touch the ground and support the body to prevent falling over. Therefore, ZMP can be considered as an excessive sufficient condition.

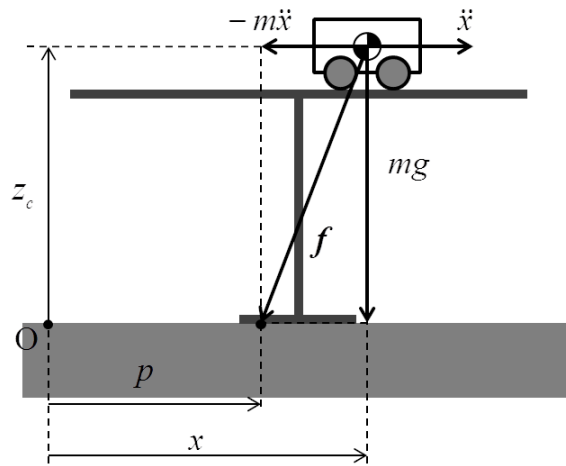
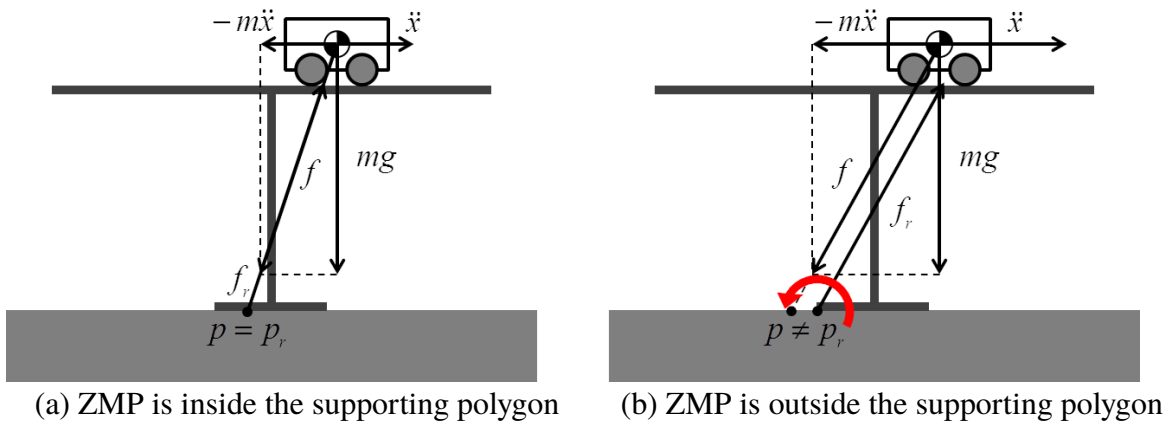


Fig. 2.3 Table-cart model



(a) ZMP is inside the supporting polygon (b) ZMP is outside the supporting polygon

Fig. 2.4 Effect of ZMP on stambling

Chapter 3

Review on Conventional Studies

In this chapter, conventional studies related to this study are introduced to show the present situation of the studies on walking robots. Firstly, the author's past study on motion control of a quadruped robot [24] is introduced.

Secondly, studies on energy consumption for locomotion are introduced. Hoyt and Taylor reported that a horse chooses a gait such that oxygen consumption for locomotion is suppressed. That suggests that the gait is chosen so that the energy required for locomotion for a unit distance is optimized. To explain the mechanism of the gait transition, Nishii proposed a simple analytical model for estimating energy consumption of animals' locomotion [60].

In last, studies on CPG are introduced. CPG is a kind of neural network which dominates rhythmical motion of animals. Spröwitz et al. proposed a quadruped robot that has an ability to ascend a small step [45]. The robot's locomotion is modulated by a CPG which considers phase differences among robot's legs directly. Owaki et al. proposed a CPG modulated by magnitude of ground reaction force acting on each leg [41]. The proposed CPG produced spontaneous gait transitions depending on the robot's locomotion velocity as observed in animals' locomotion.

3.1 Motion Control of Quadruped Robot Based on Inclination of Body

In this section, the author's past study [24] is introduced as an example of motion control of a quadruped robot. In this study, an inclination of robot's body is considered as an index of stable locomotion based on an assumption that keeping the body in a desired orientation provides stable locomotion even without feedback of ZMP. The robot's body is kept horizontal to avoid stumbling while swing legs touch to the ground. It is verified by simulations that the robot can achieve stable locomotion without feedback of the ZMP.

3.1.1 Robot Model and Motion Trajectory

The robot model for simulations is shown in Fig. 3.1 and parameters of the model are explained in Tables 3.1 and 3.2. The Open Dynamics Engine (ODE) was used to examine the proposed controller in this study. The ODE is a library of API for C++ language to calculate kinetics of solid bodies numerically [65]. The robot has three actuators in each leg, twelve actuators in total. The actuator is numbered from the base of each leg, and actuators 1, 2 and 3 rotate in pitch, roll and pitch directions, respectively, as shown in Fig. 3.2. These actuators are assumed to be able to generate any desired torque without magnitude limit. In addition, there is no energy loss such as viscous friction effects. The other conditions are shown in Table 3.3.

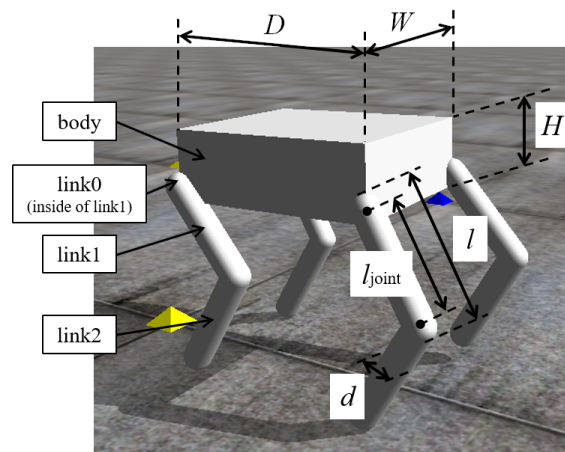


Fig. 3.1 Robot model

In this study, the gait pattern of the robot is restricted to trotting. A leg motion trajectory is determined by a ZMP trajectory and designed before the motion starts.

The desired trajectory of the center of gravity (COG) of robot's body is designed to achieve the desired ZMP trajectory and applied to designing the desired trajectory of robot's legs. The desired ZMP trajectory and trajectory of the COG are determined as explained below [66].

The origin of the world coordinates with x - and y -axis which is in the moving direction and the leftward direction to the x -axis, respectively, is fixed on the initial location of the projection point of the COG to the ground. The robot moves in a constant velocity along x -axis, and the ZMP trajectory is modified by moving in the y direction. The desired

Table 3.1 Parameters of the robot model

Symbol	Quantity	Unit
D	depth of the body	m
W	width of the body	m
H	height of the body	m
M	mass of body	kg
l	length of a link	m
l_{joint}	distance between joint axis	m
d	diameter of a link	m
m	mass of a link	kg

Table 3.2 Parameter values of the robot model

	D	W	H	M
body	0.30 m	0.24 m	0.10 m	10.0 kg
leg	l	l_{joint}	d	m
link0	-	0.00 m	0.040 m	0.30 kg
link1	0.19 m	0.15 m	0.040 m	0.30 kg
link2	0.19 m	0.15 m	0.040 m	0.30 kg

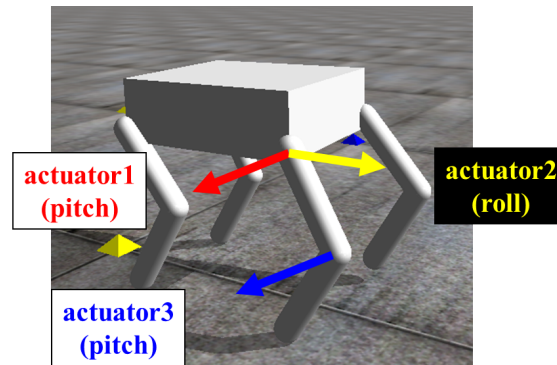


Fig. 3.2 Actuator placements of the robot model

ZMP trajectory from $t = 0$ to $t = T/4$, where T is the stride period, is shown in Fig. 3.3. The supporting line, which consists of contact points of the stance legs at the ground, is expressed as

$$y = bx \quad (3.1)$$

Table 3.3 Simulation conditions

step size	1.0×10^{-3} s
stride	0.20 m
locomotion period	1.2 s, 1.6 s
duty ratio	0.65
friction coefficient	30

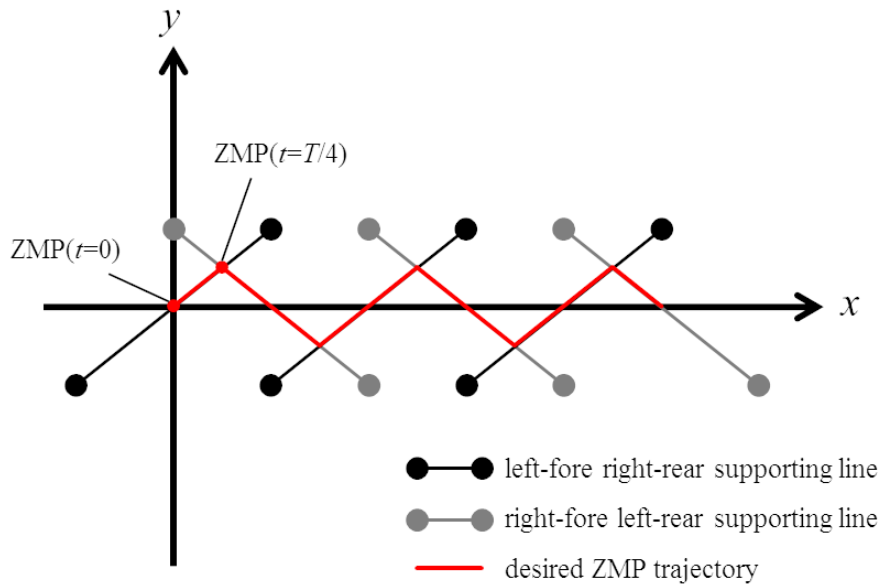


Fig. 3.3 ZMP trajectory and supporting line

where b is a constant. When the body moves in a constant velocity v along the x direction, the ZMP in the x direction corresponds to the COG in the x direction. Therefore the ZMP is on the supporting line when the following equation is satisfied;

$$x_{ZMP} = x_{COG} = vt \quad (3.2)$$

$$y_{ZMP} = bvt \quad (3.3)$$

where the subscript COG represents the parameter with respect to the COG. From the assumption that mass of legs is ignored, the relationship between the COG and the ZMP is expressed by the following equation;

$$y_{ZMP} = y_{COG} - \frac{h}{g} \ddot{y}_{COG} \quad (3.4)$$

where h and g are the distance between the COG and the ground, and the gravitational acceleration, respectively. From Eq. (3.2), (3.3) and (3.4), a second-order ordinary differential equation

$$\ddot{y}_{\text{COG}} - \frac{g}{h}y_{\text{COG}} = \frac{g}{h}bvt \quad (3.5)$$

is obtained. The general solution of 3.5 is given by

$$y_{\text{COG}}(t) = C_1 \exp\left(\sqrt{\frac{g}{h}}t\right) + C_2 \exp\left(-\sqrt{\frac{g}{h}}t\right) + bvt \quad (3.6)$$

where C_1 and C_2 are constants of integration. The velocity of the COG is given by

$$\dot{y}_{\text{COG}}(t) = \sqrt{\frac{g}{h}} \left\{ C_1 \exp\left(\sqrt{\frac{g}{h}}t\right) - C_2 \exp\left(-\sqrt{\frac{g}{h}}t\right) \right\} + bv \quad (3.7)$$

C_1 and C_2 are determined by the boundary conditions obtained from Fig. 3.3.

$$y_{\text{COG}}(0) = 0 \quad (3.8)$$

The trajectory of the COG must be smooth at $t = T/4$, i.e.,

$$\dot{y}_{\text{COG}}(T/4) = 0 \quad (3.9)$$

Therefore, C_1 and C_2 are given by

$$-C_1 = C_2 = \frac{\sqrt{\frac{h}{g}}}{\exp\left(\sqrt{\frac{h}{g}}\frac{T}{4}\right) + \exp\left(-\sqrt{\frac{h}{g}}\frac{T}{4}\right)} bv \quad (3.10)$$

The maximum displacement of the COG in the y direction is at $t = T/4$, and hence,

$$y_{\text{COGmax}} = y_{\text{COG}}\left(\frac{T}{4}\right) = C_1 \exp\left(\sqrt{\frac{g}{h}}\frac{T}{4}\right) + C_2 \exp\left(-\sqrt{\frac{g}{h}}\frac{T}{4}\right) + bv\frac{T}{4} \quad (3.11)$$

The obtained trajectory of the COG satisfies the desired ZMP trajectory.

The trajectory of the COG obtained above is applied to trajectories of stance legs to satisfy the desired trajectory of the COG. The original of the leg coordinates Σ_{leg} with x -, z - and y -axis where x is in the direction of the forward normal of frontal section of the body, z is in the direction of the downward normal of horizontal section of the body

and y is obtained as a right-handed system, respectively, is fixed on the base of each leg as shown in Fig. 3.4. From Eq. (3.7), the trajectory of the stance legs are given by the following equation:

$$y_{\text{leg}}(t) = (-1)^n \left\{ C_1 \exp\left(\sqrt{\frac{g}{h}}t\right) + C_2 \exp\left(-\sqrt{\frac{g}{h}}t\right) + bvt \right\} \quad (3.12)$$

$$\begin{cases} n = 0 & \text{for left-fore and right-hind legs} \\ n = 1 & \text{for right-fore and left-hind legs} \end{cases}$$

The trajectory of swing leg is given as a sinusoidal curve starting from $(-S/2, \pm y_{\text{COGmax}}, h - H/2)$ and reaching $(S/2, \mp y_{\text{COGmax}}, h - H/2)$ (double sign correspondence).

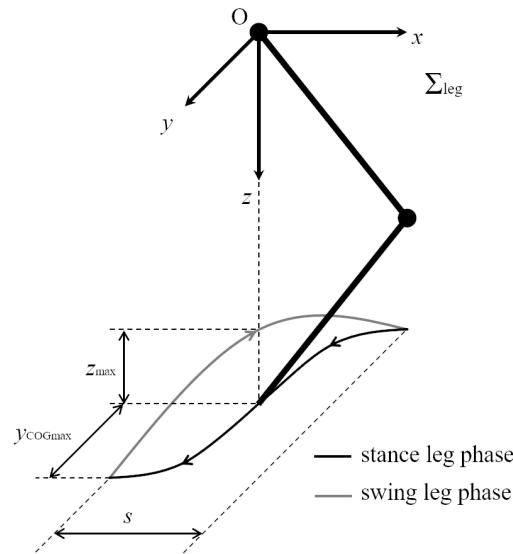


Fig. 3.4 Left-fore and right-hind leg tip trajectory

3.1.2 Controller Design based on Inclination of body

Each actuator attached to the joints of legs generates input torque to achieve the desired angle. The input torque for each joint is given by

$$\tau_i = k(\theta_{di} - \theta_i) \quad (3.13)$$

where τ_i is input torque, k is proportional gain, θ_{di} is desired angle and θ_i is measured angle, respectively. The suffix i indicates i th joint. If the input torque in Eq. (3.13) is applied to the joint motion, the links keep oscillation because there is no energy loss such as viscous friction in the actuators on the ODE. Therefore, the input torque to avoid the oscillation should be

$$\tau_i = k (\theta_{di} - \theta_i) - c\omega_i \quad (3.14)$$

where c is coefficient of viscosity and ω_i is angular velocity, respectively. The control gain k and the coefficient of viscosity c were determined by trial and error.

From the assumption that supporting legs do not slip and touch the ground at only one point, stumbling motion of the robot is restricted within rotational motion around the supporting line. Thus, it is possible to make control for avoiding stumbling easily by considering only dynamics within the vertical cross section against the supporting line as shown in Fig. 3.5. To keep the body horizontal, input torque is applied to the bases of the supporting legs (Fig. 3.6). The moment of inertia and input torque are considered as scalar variables due to the assumption on the rotational motion around the supporting line. If the inclination θ is relatively small, the equation of motion can be expressed approximately as

$$I\ddot{\theta} = \tau \quad (3.15)$$

where I is moment of inertia of the body around the line which includes the bases of the

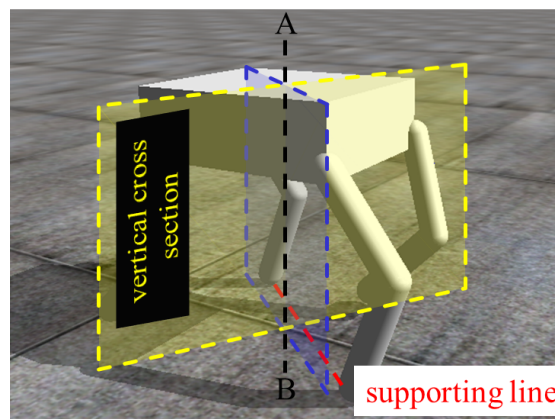


Fig. 3.5 Vertical cross section

both stance legs and τ is the input torque, respectively. The input torque τ is given by the

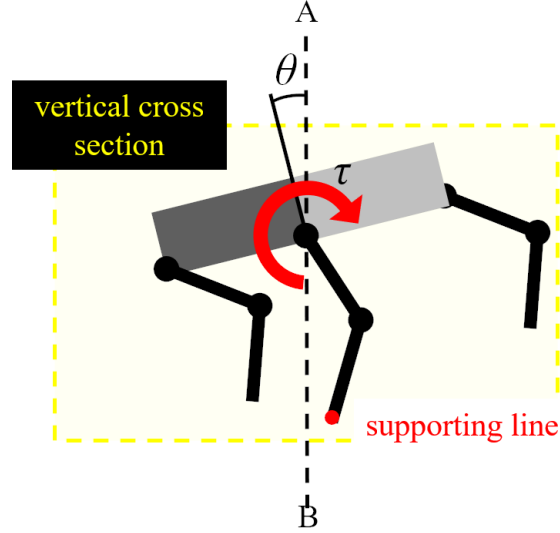


Fig. 3.6 Dynamics in the cross section

following equation;

$$\tau = -k_p\theta - k_d\dot{\theta} \quad (3.16)$$

where k_p and k_d are feedback gains. From Eq. (3.15) and (3.16), the equation of motion of the body is expressed as

$$I\ddot{\theta} + k_d\dot{\theta} + k_p\theta = 0 \quad (3.17)$$

Equation (3.17) is the equation of motion for damped oscillation. The damping ratio ζ is given by

$$\zeta = \frac{k_d}{2\sqrt{k_p I}} \quad (3.18)$$

If τ is given with the appropriate feedback gains k_p and k_d satisfying $1 < \zeta$, the body performs over damped oscillation and converges on the horizontal condition. The input torque τ obtained by Eq. (3.17) was given by the summation of τ_1 and τ_2 generated by the actuators 1 and 2, respectively, as shown in Fig. 3.7. The origin of the body coordinate Σ_{body} with x -, z - and y -axis is fixed on the COG of the body as shown in Fig. 3.8. If

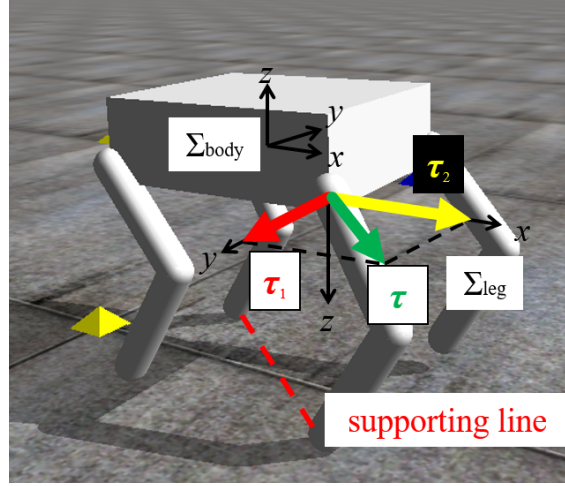


Fig. 3.7 Resultant torque model

postures of the stance legs are the same, the supporting line on Σ_{body} is given by

$$\begin{aligned} y &= bx + a \\ z &= \text{const.} \end{aligned} \quad (3.19)$$

where a is a constant. Because τ_1 and τ_2 on Σ_{leg} are in parallel with y - and x -axis on Σ_{body} respectively, the input torque τ with its magnitude τ is given as the linear combination of τ_1 and τ_2 :

$$\tau = \tau_1 + \tau_2 = |\tau_2| \mathbf{i} - |\tau_1| \mathbf{j} \quad (3.20)$$

where \mathbf{i} and \mathbf{j} are unit vectors in the x and y direction of Σ_{body} , respectively. From Eq. (3.20) and Fig. 3.8, magnitude of τ_1 and τ_2 are determined by comparison with the elements of τ , i.e.,

$$\begin{aligned} |\tau_1| &= \frac{-b}{\sqrt{1+b^2}} \tau \\ |\tau_2| &= \frac{1}{\sqrt{1+b^2}} \tau \end{aligned} \quad (3.21)$$

These equations provide a ratio to assign the input torque τ to actuators 1 and 2.

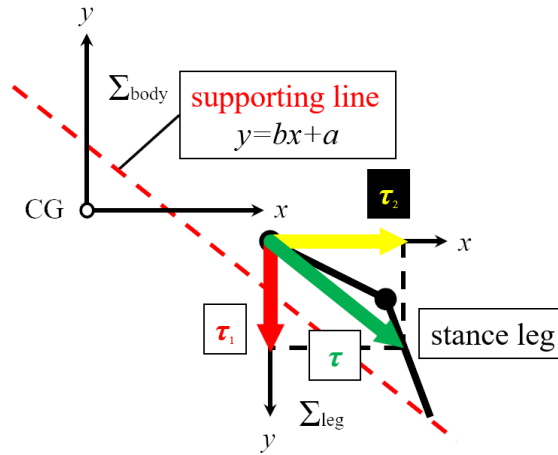


Fig. 3.8 View in the x - y plane of robot coordinates

3.1.3 Simulation Conditions and Results

The simulation was conducted to examine the effectiveness of the proposed controller design by considering the following three points :

1. Different locomotion periods that affect the stability of robot's locomotion
2. The effect of feedback gains k_p and k_d in the proposed controller
3. The dependence of stable locomotion on the ZMP

Firstly, the effect of the locomotion on the proposed controller design was examined by comparing two different locomotion periods ($T = 1.2$ s and 1.6 s). The feedback gains were set to $k_p = 500$ Nm and $k_d = 500$ Nms ($\zeta = 1.47$). Simulation on four combinations of feedback gains was conducted to determine the effective control gains under a fixed locomotion period ($T = 1.2$ s).

Then, the actual ZMP was measured in the simulation of the proposed controller with the parameters $T = 1.2$ s, $k_p = 500$ Nm and $k_d = 500$ Nms ($\zeta = 1.47$).

For all simulation, the inclination of the body around the supporting line and the ZMP were measured for three locomotion periods. With the results of the simulation on two different locomotion periods, the effect of the feedback gains and the ZMP are shown in Figs. 3.9-3.12.

As shown in Figs. 3.9 and 3.10, the proposed controller effectively reduced the inclination of the body on both simulations of different stride periods by comparison between

the result with and without feedback control. From the effect of feedback gains k_p and k_d observed in Fig. 3.11, the inclination exhibited the good performance at the damping ratio $\zeta = 1.47$.

The simulation on measurement of the ZMP in Fig. 3.12 showed the significant result. Although the actual ZMP oscillates significantly and is largely different from the desired ZMP, the robot is able to perform stable walk as shown in Fig. 3.9. This result indicates the independence of stable quadruped locomotion from the ZMP.

The controller proposed in this study restrained the inclination of the body and realized stable quadruped locomotion. In addition, it was observed that the locomotion was stable even though the ZMP trajectory was oscillated extremely and did not follow the desired trajectory.

The proposed controller was based on the assumption that the inclination is relatively small; therefore it seems difficult to avoid large inclination as shown in Fig. 3.10. Furthermore, vibration of ZMP causes a great increase of energy consumption. Because robots working outdoors are required to work with a limited power source, the energy consumption must be considered.

In conclusion, considering the inclination of the body reduced the inclination, and the robot performed stable locomotion. The possibility that the inclination can be a new index of stable locomotion was examined. However, the proposed controller may have disadvantage on avoiding larger inclination and energy consumption.

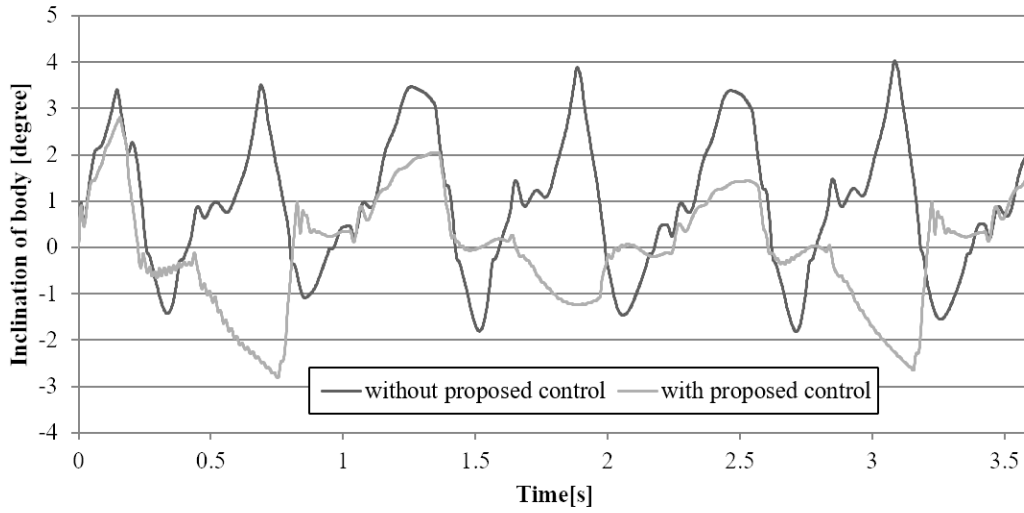


Fig. 3.9 body inclination profiles (locomotion period: 1.2 s)

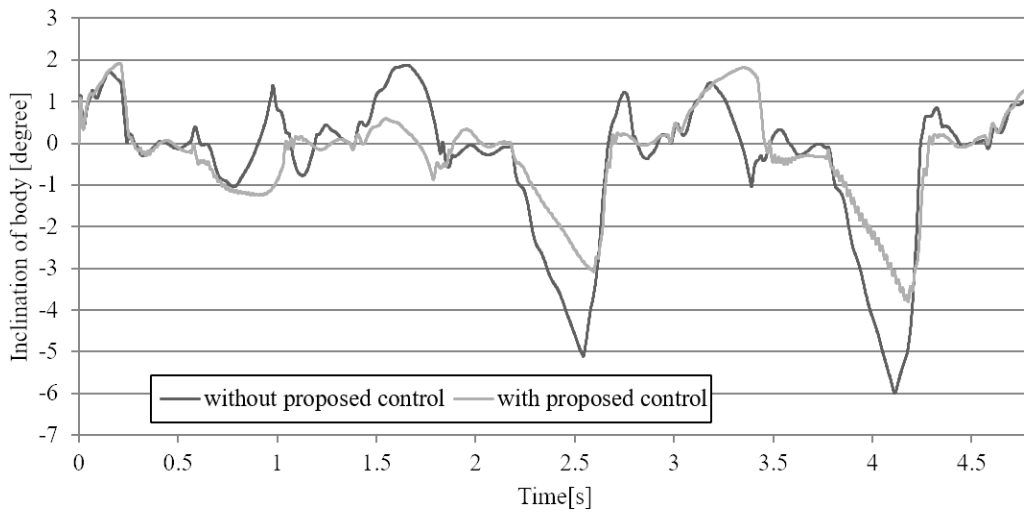


Fig. 3.10 body inclination profiles (locomotion period: 1.6 s)

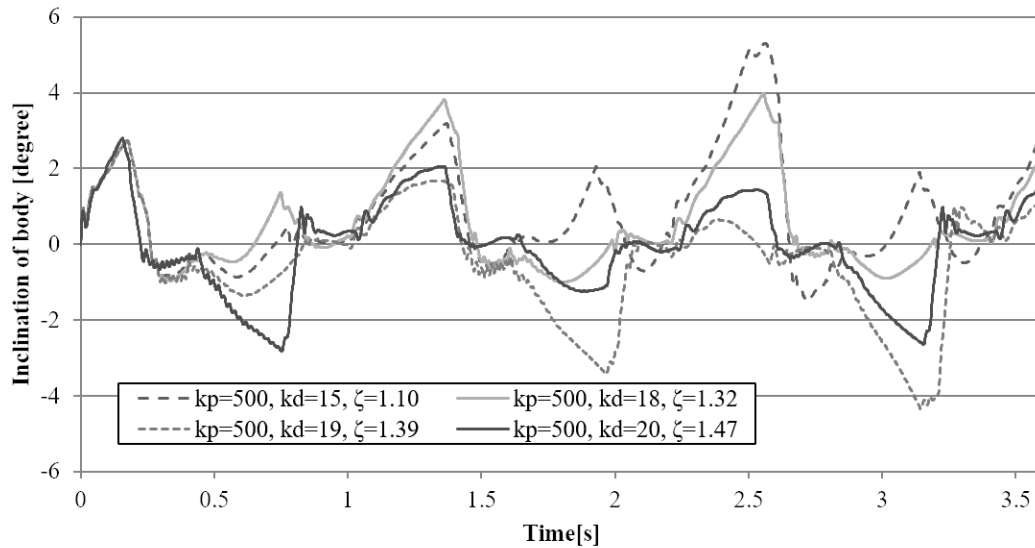


Fig. 3.11 body inclination profiles with different feedback gains (locomotion period: 1.2 s)

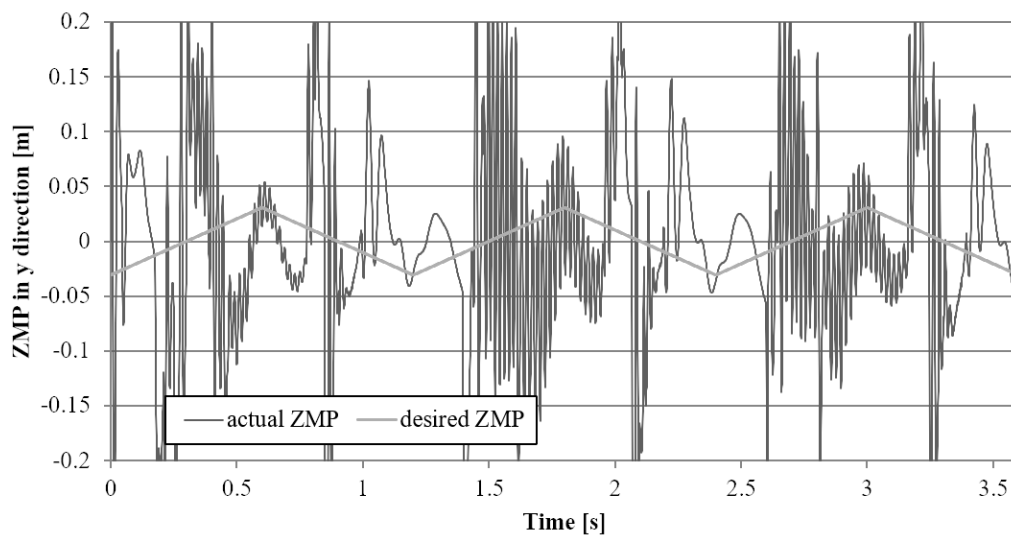


Fig. 3.12 ZMP profiles (locomotion period: 1.2 s)

3.2 Energy Consumption for Locomotion

Hoyt and Taylor measured oxygen consumption in horses during locomotion [56]. Figure 3.13 shows the oxygen consumption of horses required to move a unit distance reported in [56]. The oxygen consumption corresponds to metabolic energy consumption. As shown in Fig. 3.13, each gait has energy-optimal locomotion velocity. The horses selected the energy-optimal gait most frequently, namely, they chose less frequently the trot gait in A, the gallop gait in B, and the trot gait in C, respectively [62]. The energy consumption at the energy-optimal locomotion velocity is almost same for each gait. Moreover, it is reported that there are ranges of locomotion velocity which the horses never used for any sustained period unless they are forced to move at that locomotion velocity on a motorized treadmill. These facts suggest that the horses select the gait depending on its locomotion velocity so that the energy consumption for locomotion is optimized, yet mechanism of the optimization is unclear.

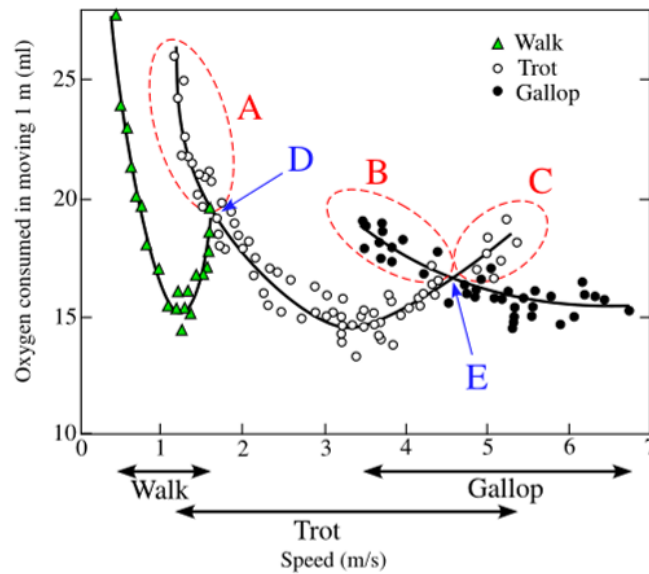


Fig. 3.13 The oxygen consumption of horses for moving a unit distance versus locomotion velocity in walk, trot and gallop gaits. Originally cited from [56], modified in [62].

Nishii proposed an analytical model for estimating energy consumption of animals' locomotion and revealing the mechanism of the optimization of the energy consumption by the gait transition. The proposed model consists of a single leg link [60] as shown in Fig. 3.14.

According to the COT profile obtained from the proposed model, it is suggested that the energy consumption for locomotion is composed of mechanical work for motion of legs and heat loss due to generating force/torque in actuators such as muscles, and the energy-optimal locomotion parameters such as duty ratio and stride length are determined by the balance of those two factors as illustrated in Fig. 3.15.

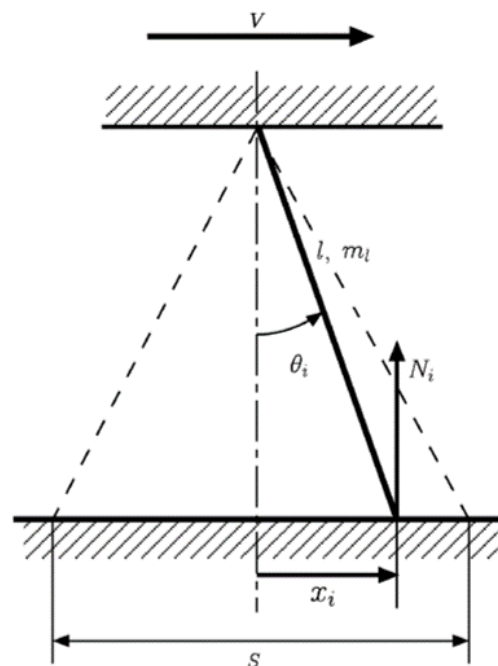


Fig. 3.14 A simple leg model [60]

The COT computed according to the model in Fig. 3.14 versus locomotion velocity obtained from typical duty ratio is shown in Fig. 3.16. Here, it is assumed that ground reaction force N_i is given by total mass of the model M divided by an average number of the stance legs, i.e., $N_i = M/n\beta$ where n is a number of legs and β is duty ratio. The solid line shows the least COT given by the optimal duty ratio.

Furthermore, Nishii derived the optimal duty ratio by two advanced methods considering more practical assumption on the ground reaction force. The first assumption (assumption 1) is that the ground reaction force is given by the total mass divided by the number

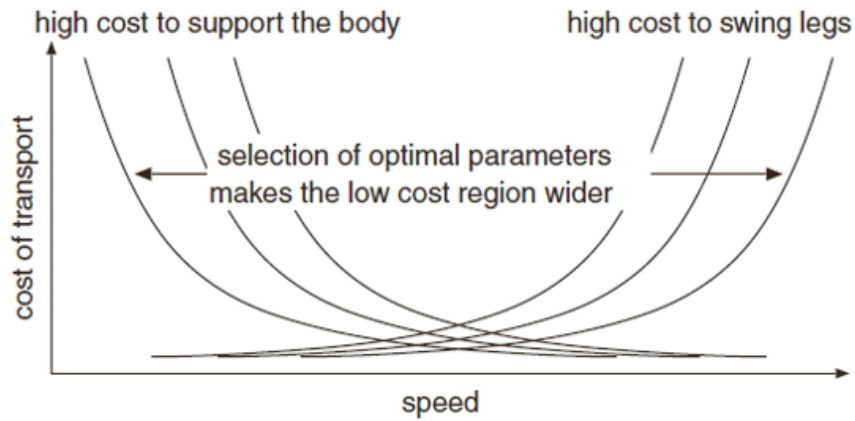


Fig. 3.15 Schematic representation of cost of transportation. Heat loss to support the body is dominant at lower locomotion velocity and mechanical work is dominant at higher locomotion velocity [60].

of the stance legs at the instance n^{st} , i.e., $N_i = M/n^{\text{st}}(t)$. In the second assumption (assumption 2), the balance of the force around the body derived by the pseudo-inverse matrix is considered. The optimal duty ratio computed on these two assumptions are shown in Fig. 3.17. As shown in Fig. 3.17, it is observed that the optimal duty ratio does not change in some ranges on the both assumptions. Similarly, the discrete change of the optimal duty ratio is observed, that is observed in the actual animals' locomotion. Those phenomena are not observed on the assumption that the ground reaction force is always evenly distributed to each leg. Nishii concluded that the distribution of the ground reaction force determined by body structure would yield a different optimal set of gait patterns.

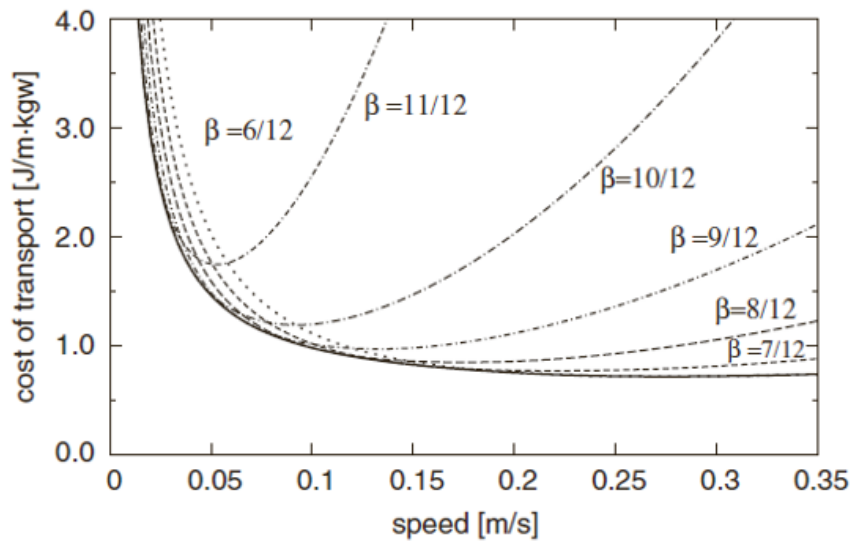


Fig. 3.16 Cost of transportation for typical duty ratio values [60].

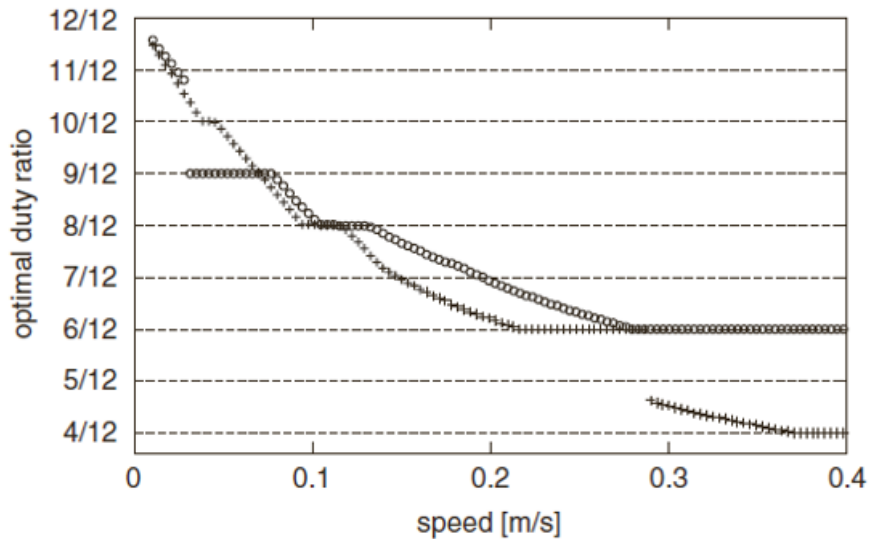


Fig. 3.17 Optimal duty ratio computed on the assumption 1 denoted by “+” and assumption 2 denoted by “o” [60].

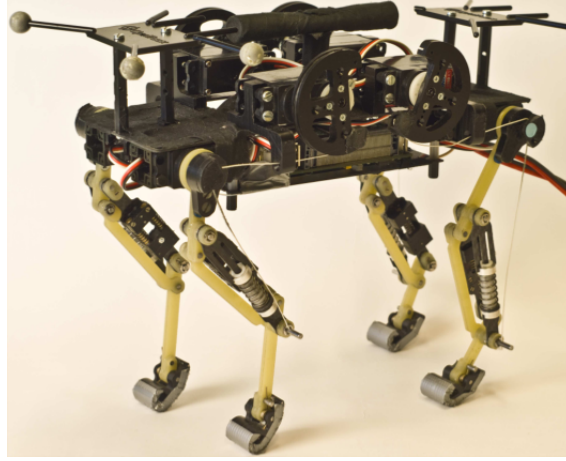


Fig. 3.18 Cheetah-cub [45]

3.3 Central Pattern Generator

locomotion is controlled in part by a distributed neural network called the “central pattern generator” (CPG) in the animals’ spinal cord.

Spröwitz et al. designed a quadruped robot named “Cheetah-cub” shown in Fig. 3.18, which is controlled by a CPG algorithm [45]. The proposed CPG regulates phase differences among legs directly, expressed by the following equation;

$$\dot{\phi}_i = 2\pi f + \sum_{j \neq i} k_{i,j} \sin(\phi_j - \phi_i - \psi_{i,j}) \quad (3.22)$$

where ϕ_i and ϕ_j are phase of the i -th and j -th oscillator, respectively, f is locomotion frequency, $k_{i,j}$ is a constant gain, and $\psi_{i,j}$ is a desired phase difference between i -th and j -th oscillator. Equation (3.22) compensates the phase differences when periodical coordination of leg motion for locomotion is disturbed. The proposed CPG successfully compensated the disturbed phase differences when ascending or descending a step and achieved stable fast locomotion.

Owaki et al. proposed a simple algorithm based on the CPG which contains phase oscillators modulated by magnitude of ground reaction force in each leg and implemented it into a quadruped robot named “Oscillex 3” shown in Fig. 3.19 [41]. They pointed out that no past study based on CPG has succeeded to reproduce gait transitions from low to high locomotion velocity using a quadruped robot and this is because most relevant research has been either completely or partly based on preprogrammed neural network

topologies in CPGs. The phase oscillators designed by them are not connected to each other by predefined connections nor preprogrammed relationship, but interact to each other physically, i.e., through force/torque distribution such as ground reaction force. The designed CPG is formulated by the following simple equation;

$$\dot{\phi}_i = \omega - \sigma N_i \cos \phi_i \quad (3.23)$$

where ϕ_i is the oscillator phase, ω is intrinsic angular velocity, σ is the weight of local sensory feedback and N_i is the ground reaction force which is detected using a pressure sensor on each foot. The mechanism of Owaki's CPG is simple: The phase oscillator tries to remain in stance phase when the ground reaction is large as shown in Fig. 3.20.

The proposed CPG successfully produced spontaneous gait transitions depending on the robot's locomotive speed which is similar to ones observed in the actual animals' locomotion. Moreover, it is shown that the gait transition optimized energy consumption for locomotion as shown in Fig. 3.21. The profile of the COT shown in Fig. 3.21 looks quite similar to the oxygen consumption profile shown in Fig. 3.13 in Hoyt and Taylor's study [56], that suggests that the CPG modulated by the ground reaction force most likely explains the mechanism of the gait transition, yet the relation between the ground reaction force and the energy consumption is not clearly explained.

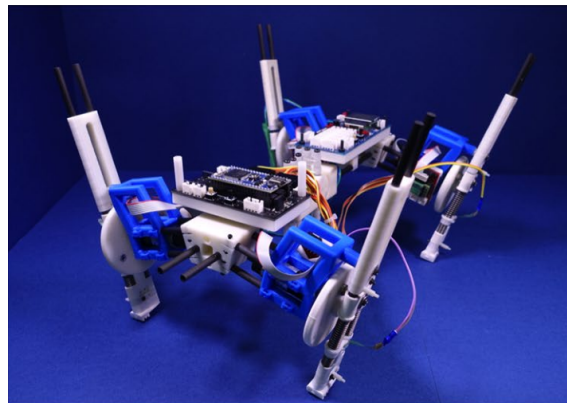


Fig. 3.19 The quadruped robot, Oscillex 3 [41]

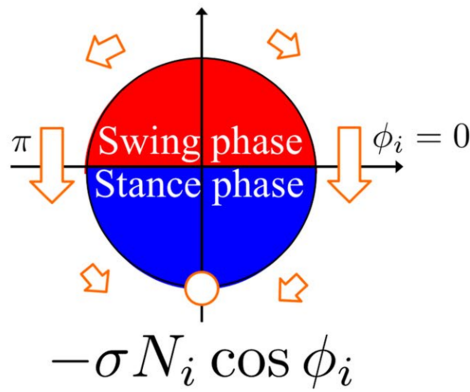


Fig. 3.20 The feedback effect on the oscillator phase [41]

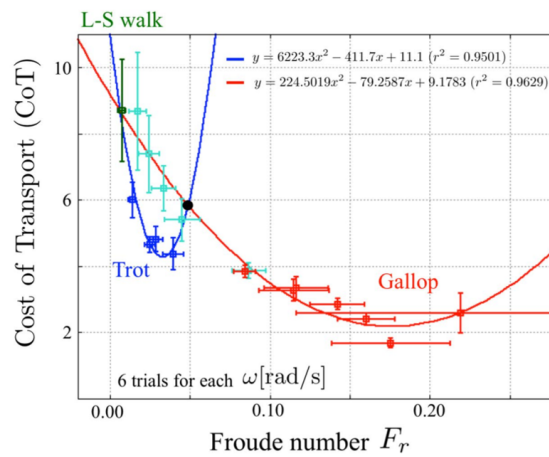


Fig. 3.21 Cost of transport versus Froude number F_r for each value of ω [41]. The Froude number is a dimensionless number proportional to locomotion velocity.

Chapter 4

Estimation of Energy Consumption

4.1 Introduction

In this section, “2-link 2-leg model” for estimating energy consumption for quadruped locomotion is proposed. In this model for quadruped locomotion, the fore legs and torso are considered and the effect of the hind legs is treated as disturbance to the torso link and this brings a biped robot model which is supported by virtual reaction force of the opposite legs. The legs are composed of two links that are sufficient approximation of actual robots’ leg structure. The advantage of the proposed model lies in the similarity to actual robots’ leg structure compared to the conventional study [60]. The proposed model is sufficiently simple for analyzing effects of the locomotion parameters, whereas essential structure of knee joints in actual robots holds and the model can be extended to other body structure types such as hexapod robots by assuming additional external disturbance force.

4.2 Simulation of Energy Consumption

4.2.1 Dynamics Model

Because the three-dimensional motion dynamics of the robot is complex, it is often assumed that motion around the roll axis, in the frontal plane, and motion around the pitch axis, in the sagittal plane, can be treated separately. In this study, we derived the dynamics of sagittal plane motion.

The friction magnitude is sufficient at the contact point between the stance leg and the ground for contact point slippage to be considered negligent. Hence, the tip of the stance leg is assumed to be pinned with a free hinge joint at the contact point. The support force provided by the hind legs is treated as a force applied to the tip of the torso link to keep the posture of the torso link.

The notations are as follows: θ_i , $i = 1 \cdots 4$: relative angle of the corresponding joint, measured by an encoder attached to each joint; θ_0 : absolute angle of the shin of the stance leg from the vertical axis; τ_i : input torque to corresponding joints; L_{sh} : length of the shin

link, L_{th} : length of the thigh link, L_{hp} : length of the torso link; L_{shG} : length from the knee to the center of gravity (COG) of the shin link; L_{thG} : length from the hip to the COG of the thigh link; L_{hpG} : length from the hip to the COG of the torso link. Each link has the following parameters: M_{sh} : mass of the shin link; M_{th} : mass of the thigh link; M_{hp} : mass of the torso link; I_{sh} : moment of inertia of the shin link around its COG; I_{th} : moment of inertia of the thigh link around its COG; I_{hp} : moment of inertia of the torso link around its COG. The corresponding shin and thigh links of the left and right legs have the same length, mass, and moment of inertia. The coordinate frame is based on the right-hand rule. The angle, angular velocity, and torque vectors are defined as follows:

$$\Theta = [\theta_0 \ \theta_1 \ \theta_2 \ \theta_3 \ \theta_4]^T \quad (4.1)$$

$$\Omega = [\omega_0 \ \omega_1 \ \omega_2 \ \omega_3 \ \omega_4]^T \quad (4.2)$$

$$\tau = [0 \ \tau_1 \ \tau_2 \ \tau_3 \ \tau_4]^T \quad (4.3)$$

The support force provided by the hind legs and applied to the tip of the torso link is defined as follows:

$$\mathbf{f} = \begin{bmatrix} f_x \\ f_z \end{bmatrix} \quad (4.4)$$

Consequently, the following dynamics are obtained:

$$M(\Theta) \dot{\Omega} + C(\Theta, \Omega) + G(\Theta) = \tau + J^T(\Theta) \mathbf{f} \quad (4.5)$$

where $M(\Theta)$ is the inertial matrix, $C(\Theta, \Omega)$ is the nonlinear torque vector including centrifugal force terms, $G(\Theta)$ is the gravitational torque vector, τ is the input torque vector and $J(\Theta)$ is the Jacobian matrix from the tip of the stance leg to the point at which the support force is applied. The second term on the right side of the equation describes the distribution of the support force vector to each joint as torque by the transpose of the Jacobian matrix to satisfy the torque constraints of each joint.

4.2.2 Simulation Conditions

In simulation, effects of locomotion parameters such as duty ratio on the mechanical work e_m and heat loss e_h were evaluated.

The locomotion parameters are determined according to the equation of the locomotion parameters (Eq. (2.1)). In the simulation, the locomotion velocity v is set to 0.10 to 0.40

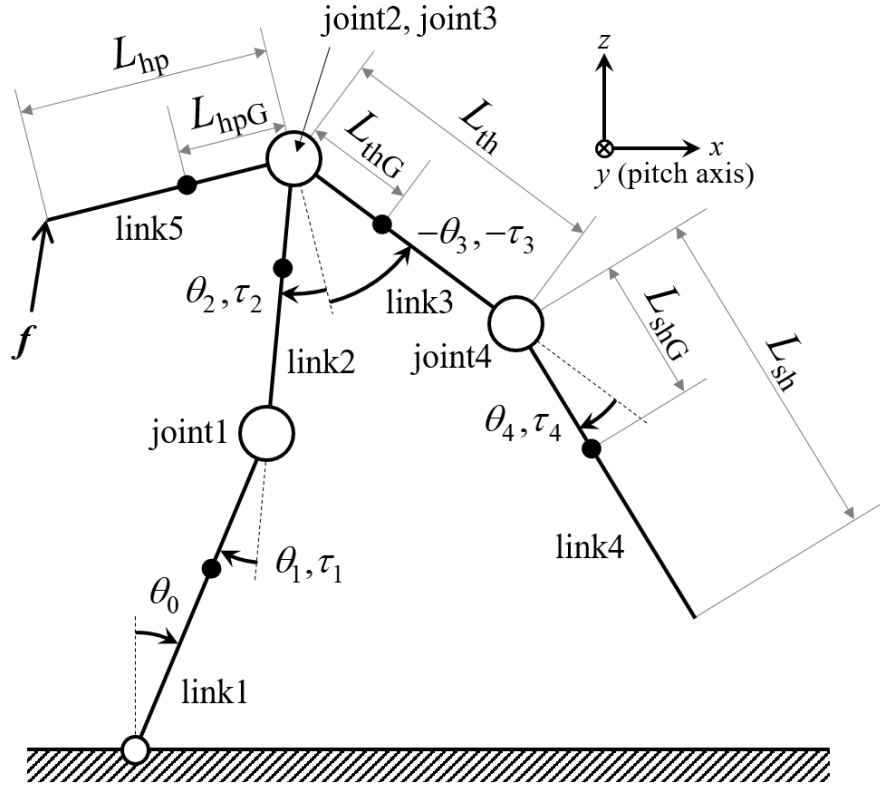


Fig. 4.1 Dynamics model for estimation of energy consumption

m/s for each 0.01 m/s and duty ratio β is set to 0.55 to 0.85 for each 0.02. The stride length s is fixed at 0.12 m. The locomotion period T is regarded as a dependent parameter.

The leg tip trajectory is given by the following equations in leg coordinate frame with origin at the hip joint axis:

$$\begin{aligned}
 \mathbf{p}(\phi) &= \begin{bmatrix} p_x(\phi) \\ p_z(\phi) \end{bmatrix} \\
 &= \begin{cases} \mathbf{p}_{\text{stance}}(\phi) & \text{for } 0 \leq \phi < \beta \\ \mathbf{p}_{\text{swing}}(\phi) & \text{for } \beta \leq \phi < 1 \end{cases} \quad (4.6)
 \end{aligned}$$

Table 4.1 Parameter values for simulation

Parameter	Value	Parameter	Value
M_{sh}	0.300 kg	L_{sh}	0.190 m
M_{th}	0.300 kg	L_{th}	0.190 m
M_{hp}	10.0 kg	L_{hp}	0.300 m
I_{sh}	0.409 kgm ²	L_{shG}	0.0950 m
I_{th}	0.201 kgm ²	L_{thG}	0.0950 m
I_{hp}	0.100 kgm ²	L_{hpG}	0.150 m

$$\mathbf{p}_{stance} = \begin{bmatrix} -\left(\frac{\phi}{\beta} - \frac{1}{2}\right)s \\ -z_0 \end{bmatrix} \quad (4.7)$$

$$\mathbf{p}_{swing} = \begin{bmatrix} \left(\frac{\phi-\beta}{1-\beta} - \frac{1}{2}\right)s \\ -z_0 + z_{max}\sin\left(\frac{\phi-\beta}{1-\beta}\pi\right) \end{bmatrix} \quad (4.8)$$

where \mathbf{p}_{stance} and \mathbf{p}_{swing} are leg tip trajectory in stance and swing phase, respectively, $\phi = \frac{1}{T}\text{mod}(t, T)$ is phase of the locomotion. z_0 is height of the leg in stance phase. The leg tip reaches at the highest point z_{max} at the middle of the swing phase.

The parameters of the dynamics model are shown in Table 4.1. The constant coefficient c is assumed to be 1 in the simulation because it depends on actuators used for an actual robot.

4.2.3 Simulation Results

The simulation results of the energy consumption are shown in Fig. 4.2 and 4.3. The color deepens as the duty ratio increases. The results show that the mechanical work increases monotonically as the locomotion velocity and duty ratio increase, whereas the heat loss has downward-convex tendency and the bottom of COT depends on the duty ratio. The increase of the heat loss in higher locomotion velocity and duty ratio is because of the fast leg motion in swing phase.

The tendency of the mechanical work and heat loss obtained in the simulation is similar to the results in the conventional study [60], thus the proposed model holds validity for estimating energy consumption.

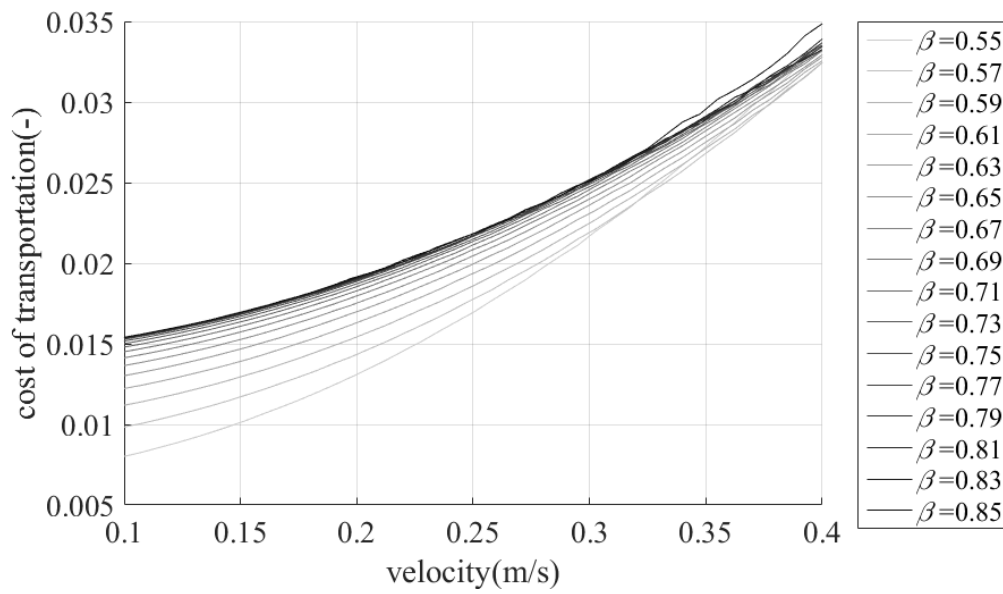


Fig. 4.2 Simulation results of COT (mechanical work)

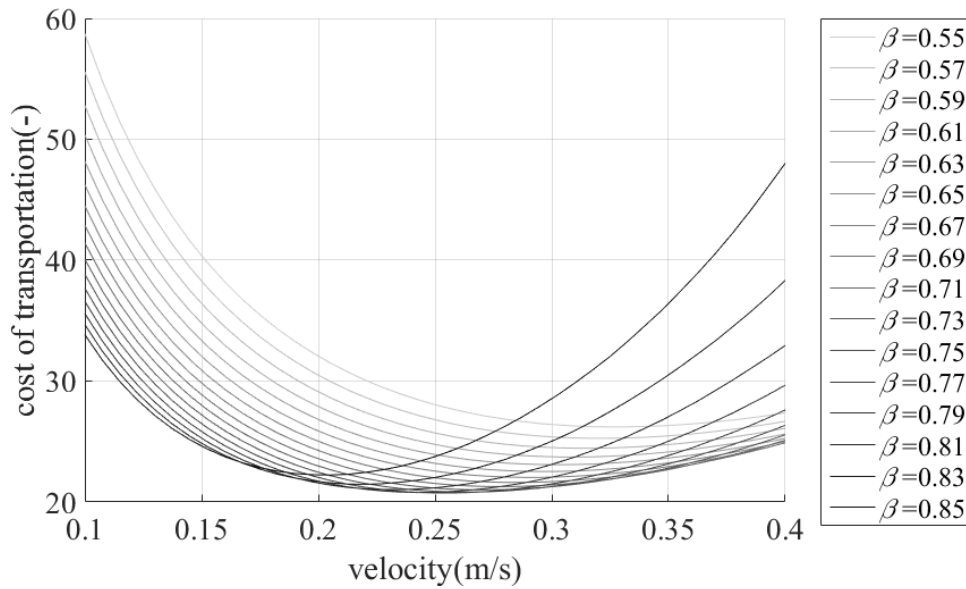


Fig. 4.3 Simulation results of COT (heat loss)

4.3 Experimental Validation of Proposed Model

4.3.1 Robot Design and Experimental Conditions

An experimental quadruped robot in Fig. 4.4 was designed to evaluate energy consumption for locomotion. This robot has two pitch motion actuators at the hip and knee joints of each leg and one roll motion actuator at the hip joint, in total twelve actuators. The parameters and features of the experimental robot are shown in Table 4.2.

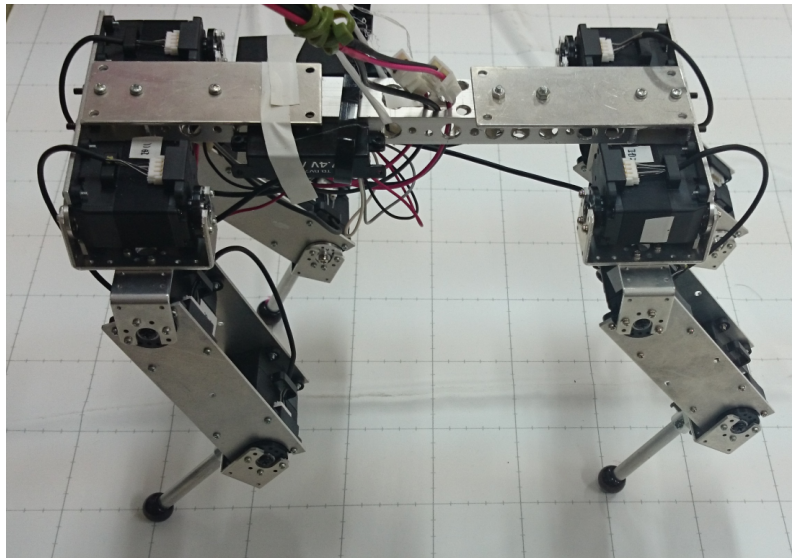


Fig. 4.4 Experimental robot

Table 4.2 Parameters and features of the experimental robot

Parameter	Value/Feature
body length	0.265 m
body width	0.15 m
length of link1	0.043 m
length of link2	0.10 m
length of link3	0.11 m
weight	1.45 kg
power source	stabilized DC power supply 11.1 V
actuators	RS405CB

In the experiments, the robot walked for one minute and the power consumption of the robot was measured. Because of the limitation of the leg tip velocity of the robot, the locomotion velocity v is set to 0.010 to 0.040 m/s for each 0.010 m/s and duty ratio β is set to 0.76 to 0.86 for each 0.02. The stride length s is fixed at 0.10 m. The locomotion period T is regarded as a dependent parameter calculated by Eq. (2.1). z_0 and z_{\max} are set to 0.22 m and 0.020 m, respectively.

4.3.2 Experimental Results

The experimental results are shown in Fig. 4.5. The results show the the COT decreases as the velocity increases. As the robot walks slowly and the heat loss is dominant at lower locomotion velocity, the experimental results are reasonable. However, the COT hardly differs as the duty ratio increases. This is because the range of the duty ratio is not sufficiently large.

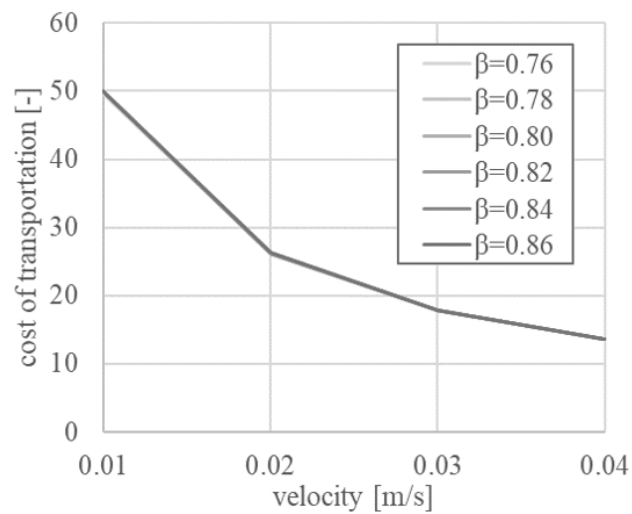


Fig. 4.5 Experimental results of energy consumption

4.3.3 Discussion

This study proposed a new dynamics model for estimating energy consumption of quadruped robots to reveal the mechanism of energy consumption for quadruped locomotion. For analytical estimation with sufficient similarity to actual robots' leg structure, a simplified dynamics model of a quadruped robot was derived. The simulation results were verified by the experiments and the experimental results showed the energy consumption profiles as estimated by the simulation. Therefore the proposed model holds generality of energy consumption for legged-locomotion results whereas the proposed model considers only half of the quadruped robot's body.

Chapter 5

Estimation of Disturbance and Ground Reaction Force

5.1 Disturbance Observer for Estimating Disturbance Force of a Biped Robot

5.1.1 Introduction

In the author's study [67], it is proposed to apply the 2-link 2-leg model for a disturbance observer to estimate disturbance acting on a walking robot.

In this section, a biped robot developed by Uchiyama et al. [83] is considered for the design of the basic structure of the disturbance observer because it has a suitable structure for examining the effectiveness of the proposed dynamics model and the performance of the disturbance observer.

The biped robot shown in Fig. 5.1 is designed originally for supporting object transportation up the stairs [83]. This robot has four pitch motion actuators for the hips and knees of each leg; roll and yaw motions are conducted by a human operator. Figure 5.2 shows the assembled robot and its three-view drawing, in which knees are driven by actuators in the hip through timing belts to reduce the inertia in leg movements. The robot has a height (h) of 0.96 m, width (w) of 0.60 m, and total mass of 10 kg.

The robot's artificial legs, which were originally designed for strenuous athletic movement, are made of Carbon-fiber-reinforced plastic and provide flexibility and adequate strength. Hence, the developed robot may be used in an actual rough terrain environment. The center of gravity (COG) of the robot is located at the point where the foot contacts the ground, considering the round shape of the artificial leg and balance of the robot in the standing state.

The transportation of objects is a common industrial task which is often undertaken by forklifts, turret trucks, and unmanned autonomous vehicles to increase working efficiency and more efficiency is required considering lack of workers in the transportation field

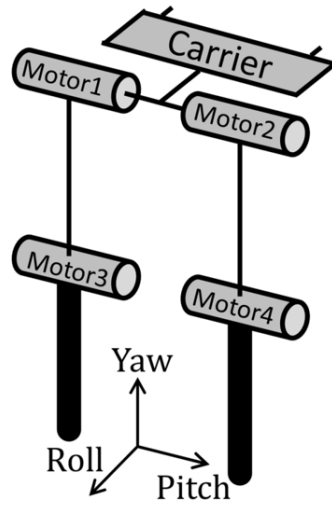


Fig. 5.1 Proposed robot for transportation of objects

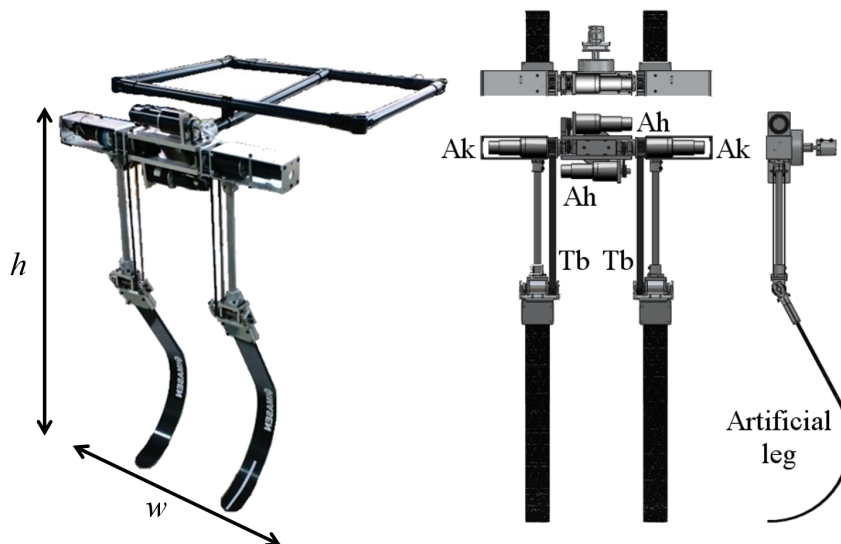


Fig. 5.2 Robot system. Left: photo. Right: three-view drawing, Ah: actuator for hip, Ak: actuator for knee, and Tb: timing belt [83]

nowadays. Similarly, transportation systems consisting of simple and inexpensive equipment, such as shopping carts and handcarts, are widely used in many fields. These types of equipment are not driven by actuators but directly by human operators and are mostly used on even floors or terrain because wheels are not suitable for steps, stairs, and rough terrain. The crawler cart with an internal combustion engine, developed for agricultural tasks, is commercially available and can be used on rough terrain [68]. It is able to ascend a step of up to approximately 0.1 m, which is not sufficient to achieve the climbing of stairs.

Equipment with legs can ascend higher steps, compared to equipment with wheels and crawlers. Sano et al. proposed a legged transportation system based on passive biped walking [69], which can be used on rough terrain. As its walking mechanism is passive and it does not use any actuator, it is inexpensive and can be implemented both in industrial and residential setting. However, such systems cannot transport objects up the stairs, because the climbing step size is 0.15 m. In addition, a problem of “knee folding” arises when climbing uphill. For uncertain terrain and smooth walking, many biped robot systems have been studied. These studies focus on the ability to walk stably, despite unevenness and uncertainty in the terrain, using leg-wheel combinations [70], foot systems maintaining four contact points with the ground [71], landing pattern modification [72], compliant mechanisms with artificial muscles [73], kinodynamic gait planning [74], tracking control to zero-moment-point reference using flat rectangular soles with force sensors at each corner [75], passive dynamic walking [76, 77], new sole mechanisms [78], three-dimensional walking [79] and flexible foot structure [80, 81]. Other studies on biped robots focus on smoothing of the walking motion, such as trajectory generation for direction turning [82].

As mentioned above, a transportation task is usually undertaken by human operators and mechanical equipment. Walking robots are suitable to working on rough terrain. These facts suggest the necessity for human-operated walking robots. For such human-robot collaboration systems, the recognition of human intention/command is critical for controlling the robot appropriately.

Considering the possibility of practical implementation, we reported a new human-operated mobile biped system, which uses actuators for transporting objects up stairs or high steps [83]. The legs of the proposed robot were composed of artificial legs meant for athletes because of their strength and flexibility. The robot successfully climbed the stairs with a simple PID controller and human operation; however, the previous study did not

consider the support force and torque applied by the operator to simplify the problem.

In this section, a disturbance observer for estimating disturbance torques given to a human-operated biped robot is proposed. The disturbance observer is designed under the assumption that a human operator applies a support force to the robot as disturbance to each joint. First, the dynamics of the robot system is derived to conduct a simulation for investigating the performance of the proposed observer. Then, the observer is designed based on a high-gain structure. With the obtained dynamics, it is theoretically proven that the observer could estimate the disturbance with sufficient accuracy by choosing observer gains appropriately. Finally, simulation results demonstrate the effectiveness of the observer.

5.1.2 Dynamics Model

To design the disturbance observer, the robot's dynamics is derived. The 2-link 2-leg model shown in Fig. 4.1 in chapter 4 is adopted as the dynamics of the biped robot. In addition to the assumptions that are considered in the previous chapter, it is assumed that each link is rigid; therefore, the flexibility of the artificial leg is negligible. The force provided by the human operator is treated as a force applied to the tip of the hip link, instead of the support force f provided by the hid legs in Fig. 4.1. The resultant equation of motion is exactly same as the Eq. (4.5).

To design the disturbance observer, the system's state space equation is derived. A state vector \mathbf{x} , input vector \mathbf{u} and output vector \mathbf{y} are defined as follows:

$$\mathbf{x} = \begin{bmatrix} \mathbf{x}_1 \\ \mathbf{x}_2 \end{bmatrix} = \begin{bmatrix} \Theta \\ \Omega \end{bmatrix} \quad (5.1)$$

$$\mathbf{u} = \boldsymbol{\tau} \quad (5.2)$$

$$\mathbf{y} = \mathbf{x}_1 \quad (5.3)$$

where \mathbf{x}_1 and \mathbf{x}_2 are the state variables. The dynamics are converted into the state space

form:

$$\begin{aligned}\dot{\boldsymbol{x}} &= \begin{bmatrix} \dot{\boldsymbol{x}}_1 \\ \dot{\boldsymbol{x}}_2 \end{bmatrix} \\ &= \begin{bmatrix} \boldsymbol{M}^{-1}(\boldsymbol{x}_1) \{ \boldsymbol{u} + \boldsymbol{J}^T(\boldsymbol{x}_1) \boldsymbol{f} - \boldsymbol{C}(\boldsymbol{x}) - \boldsymbol{G}(\boldsymbol{x}_1) \} \\ \boldsymbol{x}_2 \end{bmatrix} \\ &= \begin{bmatrix} \boldsymbol{x}_2 \\ \boldsymbol{\xi}(\boldsymbol{x}, \boldsymbol{u}, \boldsymbol{f}) \end{bmatrix} \end{aligned} \quad (5.4)$$

$$\boldsymbol{y} = [\boldsymbol{I}_5 \ \mathbf{0}_{5 \times 5}] \boldsymbol{x} \quad (5.5)$$

where $\boldsymbol{\xi}(\boldsymbol{x}, \boldsymbol{u}, \boldsymbol{f})$ corresponds to $\dot{\boldsymbol{x}}_2$, \boldsymbol{I}_n is the $n \times n$ identity matrix, and $\mathbf{0}_{n \times m}$ is the $n \times m$ zero matrix, respectively.

5.1.3 Observer Design

The support force \boldsymbol{f} , applied by an operator, is distributed to each joint by the Jacobian matrix \boldsymbol{J} . The distributed torque vector \boldsymbol{d} is defined as follows:

$$\boldsymbol{d} = \boldsymbol{J}^T \boldsymbol{f} = [d_0 \ d_1 \ d_2 \ 0 \ 0]^T \quad (5.6)$$

The resulting torque vector \boldsymbol{d} because of the support force \boldsymbol{f} contributes to supporting the robot's posture in the sagittal plane. Here, it is regarded as the disturbance to the actuators because the support force is generally unknown. The 4th and 5th elements of \boldsymbol{d} are zero, as the Jacobian matrix does not contain θ_3 or θ_4 . The roll and yaw motions conducted by the operator cause torques to each joint, which are not described in the proposed sagittal dynamics in Eq. (5.4) and (5.5). The disturbance torque vector, in real dynamics, includes those modeling errors and is estimated by the disturbance observer without distinguishing the disturbance source.

The disturbance torque vector is considered as one of the state variable vectors to formulate an extended state space equation for describing the entire dynamics of the robot including the disturbance vector.

$$\boldsymbol{x} = \begin{bmatrix} \boldsymbol{x}_1 \\ \boldsymbol{x}_2 \\ \boldsymbol{d} \end{bmatrix} \quad (5.7)$$

The state space equation becomes as follows:

$$\begin{aligned}\dot{\mathbf{x}} &= \begin{bmatrix} \dot{x}_1 \\ \dot{x}_2 \\ \dot{\mathbf{d}} \end{bmatrix} \\ &= \begin{bmatrix} M^{-1}(\mathbf{x}_1) \left\{ \mathbf{u} + \begin{matrix} x_2 \\ \mathbf{0}_{5 \times 1} \end{matrix} - \mathbf{C}(\mathbf{x}) - \mathbf{G}(\mathbf{x}_1) \right\} \end{bmatrix} \\ &= \begin{bmatrix} x_2 \\ \boldsymbol{\xi}(\mathbf{x}, \mathbf{u}) \\ \mathbf{0}_{5 \times 1} \end{bmatrix} \end{aligned} \quad (5.8)$$

$$\mathbf{y} = [\mathbf{I}_5 \ \mathbf{0}_{5 \times 10}] \mathbf{x} \quad (5.9)$$

Here, as the dynamics of the disturbance are unknown, the time derivative of \mathbf{d} is assumed to be $\mathbf{0}$.

To estimate the unknown torque induced by the support force of the operator, a disturbance observer was designed. In this section, a high-gain observer was considered a suitable candidate for the proposed system owing to its robustness. The high-gain observer was designed according to the following procedure [84]: By assuming that the output vector is $\mathbf{y} = \mathbf{x}_1$, the high-gain observer is described as follows:

$$\begin{aligned}\hat{\dot{\mathbf{x}}} &= \begin{bmatrix} \hat{\dot{x}}_1 \\ \hat{\dot{x}}_2 \\ \hat{\dot{\mathbf{d}}} \end{bmatrix} \\ &= \begin{bmatrix} \mathbf{H}_1(\mathbf{y} - \hat{\mathbf{x}}_1) \\ \mathbf{H}_2(\mathbf{y} - \hat{\mathbf{x}}_1) \\ \mathbf{H}_3(\mathbf{y} - \hat{\mathbf{x}}_1) \end{bmatrix} \\ &\quad + \begin{bmatrix} M^{-1}(\hat{\mathbf{x}}_1) \left\{ \mathbf{u} + \begin{matrix} \hat{x}_2 \\ \mathbf{0}_{5 \times 1} \end{matrix} - \mathbf{C}(\hat{\mathbf{x}}) - \mathbf{G}(\hat{\mathbf{x}}_1) \right\} \end{bmatrix} \\ &= \begin{bmatrix} \mathbf{H}_1(\mathbf{y} - \hat{\mathbf{x}}_1) \\ \mathbf{H}_2(\mathbf{y} - \hat{\mathbf{x}}_1) \\ \mathbf{H}_3(\mathbf{y} - \hat{\mathbf{x}}_1) \end{bmatrix} + \begin{bmatrix} \hat{x}_2 \\ \boldsymbol{\xi}_0(\hat{\mathbf{x}}, \mathbf{u}) \\ \mathbf{0}_{5 \times 1} \end{bmatrix} \end{aligned} \quad (5.10)$$

where $\boldsymbol{\xi}_0(\hat{\mathbf{x}}, \mathbf{u})$ is the nominal dynamics for x_2 , $\mathbf{H}_1 = \text{diag}(h_{11} \cdots h_{15})$, $\mathbf{H}_2 = \text{diag}(h_{21} \cdots h_{25})$ and $\mathbf{H}_3 = \text{diag}(h_{31} \cdots h_{35})$ are the observer gain matrices. The notation $\hat{\cdot}$ indicates the states estimated by the observer. With high gains \mathbf{H}_1 , \mathbf{H}_2 , and

\mathbf{H}_3 , the observer can estimate the states with sufficient accuracy. Now, the dynamics of estimation error \mathbf{e} are considered:

$$\mathbf{e} = \begin{bmatrix} \mathbf{e}_1 \\ \mathbf{e}_2 \\ \mathbf{e}_d \end{bmatrix} = \begin{bmatrix} \mathbf{x}_1 - \hat{\mathbf{x}}_1 \\ \mathbf{x}_2 - \hat{\mathbf{x}}_2 \\ \mathbf{d} - \hat{\mathbf{d}} \end{bmatrix} \quad (5.11)$$

$$\begin{aligned} \dot{\mathbf{e}} &= \begin{bmatrix} -\mathbf{H}_1 \mathbf{e}_1 \\ -\mathbf{H}_2 \mathbf{e}_1 \\ -\mathbf{H}_3 \mathbf{e}_1 \end{bmatrix} + \begin{bmatrix} \mathbf{e}_2 \\ \boldsymbol{\xi}(\mathbf{x}, \mathbf{u}) - \boldsymbol{\xi}_0(\hat{\mathbf{x}}, \mathbf{u}) \\ \boldsymbol{\delta} \end{bmatrix} \\ &= \begin{bmatrix} -\mathbf{H}_1 \mathbf{e}_1 \\ -\mathbf{H}_2 \mathbf{e}_1 \\ -\mathbf{H}_3 \mathbf{e}_1 \end{bmatrix} + \begin{bmatrix} \mathbf{e}_2 \\ \mathbf{X}(\mathbf{x}, \hat{\mathbf{x}}, \mathbf{u}) \\ \boldsymbol{\delta} \end{bmatrix} \end{aligned} \quad (5.12)$$

where $\boldsymbol{\delta}$ is the real dynamics of \mathbf{d} , and $\mathbf{X}(\mathbf{x}, \hat{\mathbf{x}}, \mathbf{u})$ is the difference between the real and nominal dynamics of \mathbf{x}_2 . By taking $\mathbf{H}_1 = \frac{1}{\varepsilon} \mathbf{A}_1$, $\mathbf{H}_2 = \frac{1}{\varepsilon^2} \mathbf{A}_2$ and $\mathbf{H}_3 = \frac{1}{\varepsilon^2} \mathbf{A}_3$ with $\mathbf{A}_1 = \text{diag}(\alpha_{11} \cdots \alpha_{15})$, $\mathbf{A}_2 = \text{diag}(\alpha_{21} \cdots \alpha_{25})$ and $\mathbf{A}_3 = \text{diag}(\alpha_{31} \cdots \alpha_{35})$ for positive constants $\alpha_{11} \cdots \alpha_{35}$ and $\varepsilon \ll 1$, the error dynamics become as follows:

$$\dot{\mathbf{e}} = \begin{bmatrix} -\frac{1}{\varepsilon} \mathbf{A}_1 \mathbf{e}_1 \\ -\frac{1}{\varepsilon^2} \mathbf{A}_2 \mathbf{e}_1 \\ -\frac{1}{\varepsilon^2} \mathbf{A}_3 \mathbf{e}_1 \end{bmatrix} + \begin{bmatrix} \mathbf{e}_2 \\ \mathbf{X}(\mathbf{x}, \hat{\mathbf{x}}, \mathbf{u}) \\ \boldsymbol{\delta} \end{bmatrix} \quad (5.13)$$

To show the effect of the observer gain, the scaled error is defined as follows:

$$\boldsymbol{\eta} = \begin{bmatrix} \boldsymbol{\eta}_1 \\ \boldsymbol{\eta}_2 \\ \boldsymbol{\eta}_d \end{bmatrix} = \begin{bmatrix} \frac{1}{\varepsilon} \mathbf{e}_1 \\ \mathbf{e}_2 \\ \mathbf{e}_d \end{bmatrix} \quad (5.14)$$

Then, the following equation is obtained:

$$\varepsilon \dot{\boldsymbol{\eta}} = \begin{bmatrix} -\mathbf{A}_1 \boldsymbol{\eta}_1 \\ -\mathbf{A}_2 \boldsymbol{\eta}_1 \\ -\mathbf{A}_3 \boldsymbol{\eta}_1 \end{bmatrix} + \begin{bmatrix} \boldsymbol{\eta}_2 \\ \varepsilon \mathbf{X}(\mathbf{x}, \hat{\mathbf{x}}, \mathbf{u}) \\ \varepsilon \boldsymbol{\delta} \end{bmatrix} \quad (5.15)$$

This equation shows that the modeling error effect $\mathbf{X}(\mathbf{x}, \hat{\mathbf{x}}, \mathbf{u})$ and $\boldsymbol{\delta}$ on the estimation error \mathbf{e} can be reduced by taking small ε .

5.1.4 Simulation Conditions

A reference trajectory for the robot was generated by assuming that the stair profile is known. The motion up the stairs was composed of four intervals as shown in Fig. 5.3. In

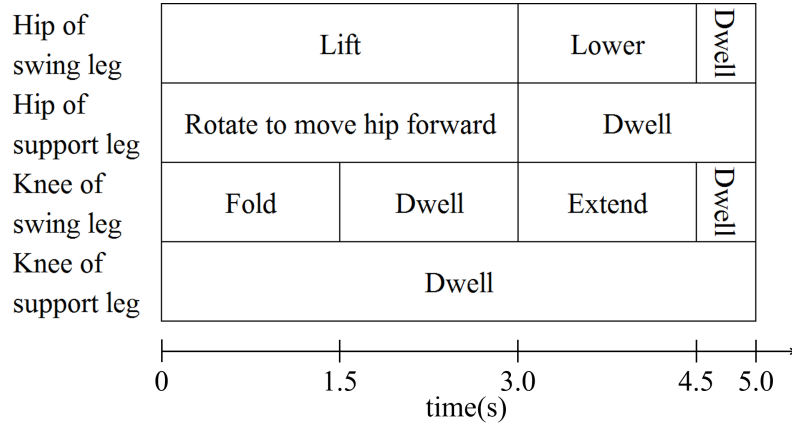


Fig. 5.3 Motion procedure for individual link

the first motion interval, the robot lifted the thigh link of the swing leg, and the shin link of the swing leg was folded. In the second interval, the robot maintained the lift motion of the swing leg, while the absolute angle of the swing leg's shin link was kept constant. During the lift motion, the support leg pulled the hip link forward. In the third interval, the thigh link of the swing leg started to lower, and the knee of the swing leg was extended until the swing leg touched the ground. In the final interval, the robot held its posture for a while. To achieve smooth motion, the following reference trajectory of the absolute angle of the links to the vertical axis was designed:

$$q_r = \frac{q_e - q_s}{2} \left\{ \sin \left(\frac{\pi t}{T} - \frac{\pi}{2} \right) + 1 \right\} + q_s \quad (5.16)$$

where q_r is the reference trajectory for each link angle, q_s is the initial angle, q_e is the end angle, t is time, and T is the motion time period from q_s to q_e . q_s , q_e and T values were varied based on the required motion at each interval. Figure 5.4 shows the resulting robot motion up the stairs at each second; the color deepens as time passes. The reference trajectory of the absolute angle was converted to the relative angle by the following coordinate transformation:

$$\Theta_r = Aq_r \quad (5.17)$$

where Θ_r is the reference trajectory vector of the relative angle, q_r is the reference trajectory vector of the absolute angle, and A is a coordinate transformation matrix. The trajectory of the relative angle is shown in Fig. 5.5.

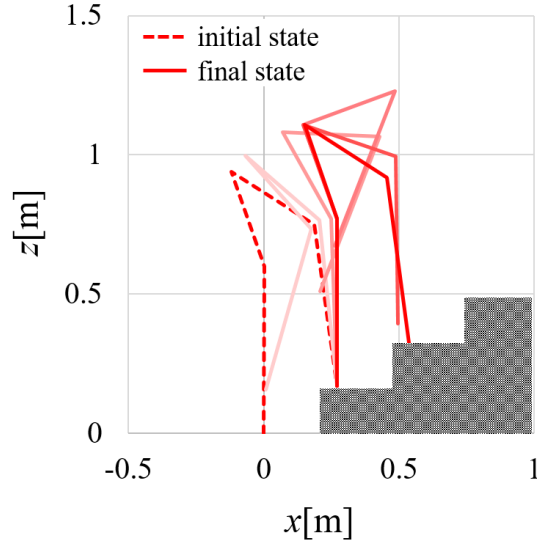


Fig. 5.4 Designed robot motion

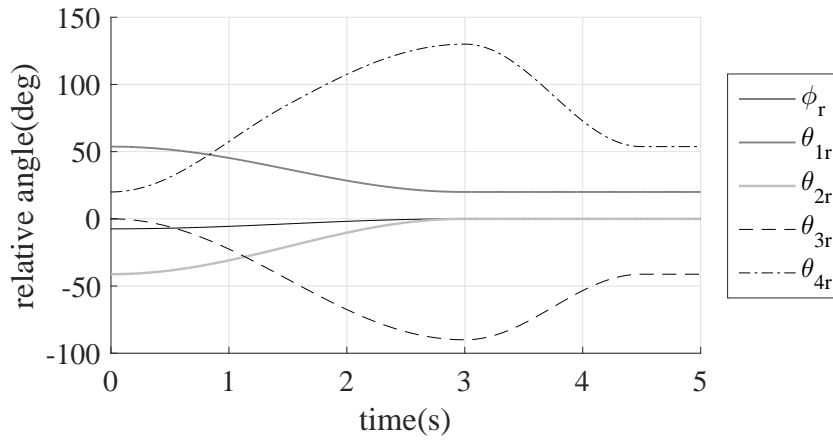


Fig. 5.5 Reference trajectory of relative joint angles

In the simulation, the support force vector of the operator was assumed to be applied to the hip link only in the horizontal direction, as the robot supported the vertical load, and the operator pushes and/or pulls the robot in horizontal direction. This leads to the following:

$$\mathbf{f} = \begin{bmatrix} f_x \\ 0 \end{bmatrix} \quad (5.18)$$

Table 5.1 Simulation conditions

Parameter	Value	Parameter	Value
Step height	0.17 m	Walking period	10 s (5 s/step)
Step width	0.27 m	Sampling period	1 ms

Table 5.2 Parameter values for simulation

Parameter	Value	Parameter	Value
M_{sh}	0.930 kg	L_{sh}	0.60 m
M_{th}	1.672 kg	L_{th}	0.36 m
M_{hp}	3.340 kg	L_{hp}	0.30 m
I_{sh}	0.409 kgm ²	L_{shG}	0.168 m
I_{th}	0.201 kgm ²	L_{thG}	0.060 m
I_{hp}	0.100 kgm ²	L_{hpG}	0.050 m

Here, it is assumed that the operator's support force f_x is applied like a PID control for the angle ϕ .

In addition, another PID control was applied to each joint to track the reference trajectory. The input torque to each joint was compensated by the observer as follows:

$$\mathbf{u} = \mathbf{u}_{PID} - \hat{\mathbf{d}} \quad (5.19)$$

where \mathbf{u}_{PID} is the input calculated by the PID controller. The PID controller and observer gains were determined by trial and error. To investigate the performance of the proposed system, including the disturbance observer, a simulation was conducted under the conditions and actual robot parameters listed in Table 5.1 and 5.2.

5.1.5 Simulation Results

The simulation results of the angular velocity and disturbance estimation are shown in Figs. 5.6-5.9. The results show that the estimation was performed well by the observer. The observer was also able to estimate the disturbance with sufficient accuracy; however, a small delay in estimation was observed owing to the modeling assumption that disturbance is constant. The observer could not track the rapid change in disturbance; however, the estimation results confirm sufficient performance for practical implementation purpose.

5.1.6 Discussion

In this section, a disturbance observer design for estimating the support force applied to a human-operated biped robot by the human operator is proposed. The dynamics for the proposed robot were modeled by assuming that the support force is considered as a disturbance to each joint. The observer was designed to estimate the disturbance based on the high-gain observer; it was proven that the observer can estimate the disturbance with sufficient accuracy. The simulation results showed that the observer successfully estimated the support force as a disturbance even though the disturbance property was completely unknown.

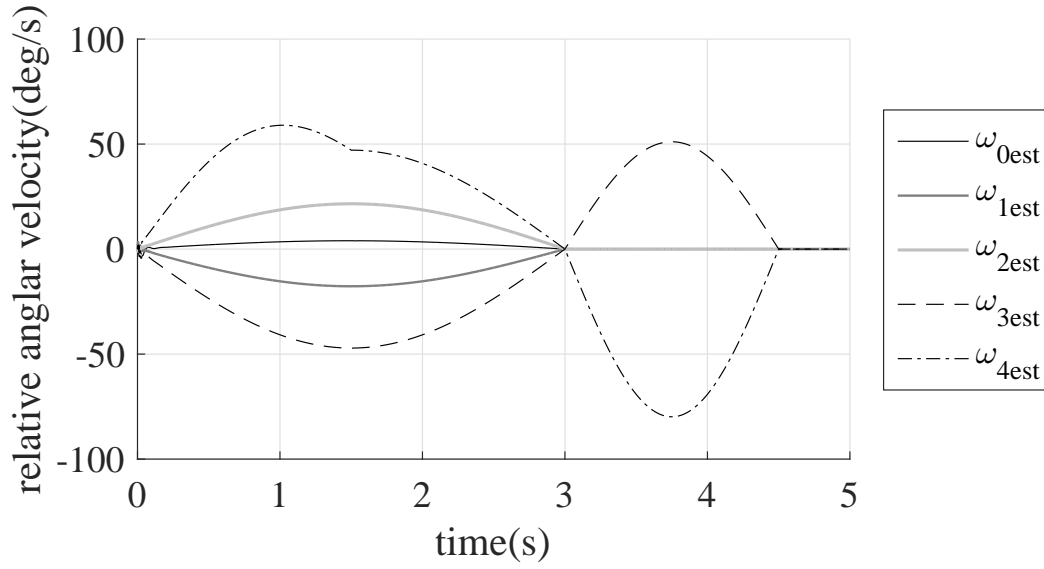


Fig. 5.6 Estimation result of relative angular velocity

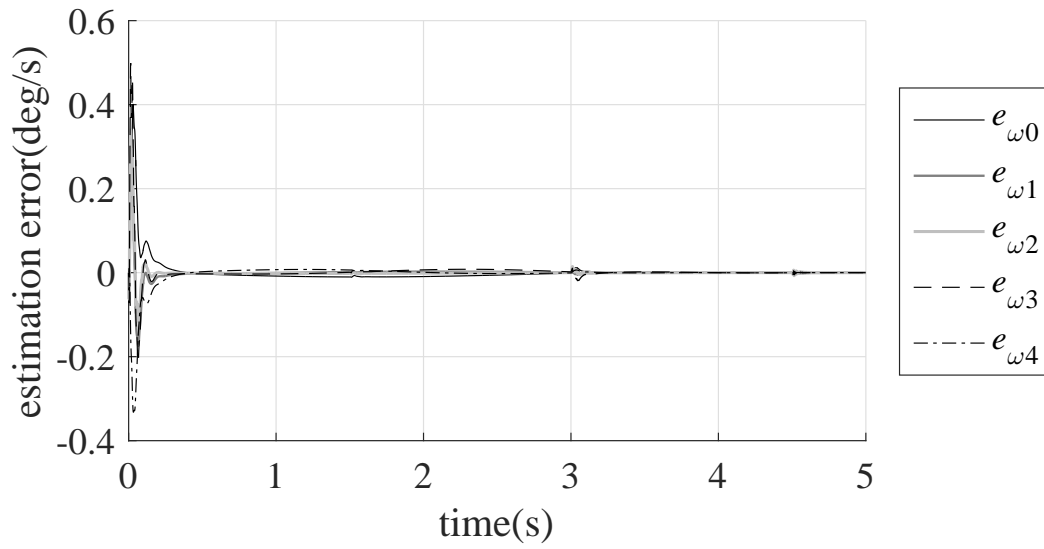


Fig. 5.7 Estimation error of relative angular velocity

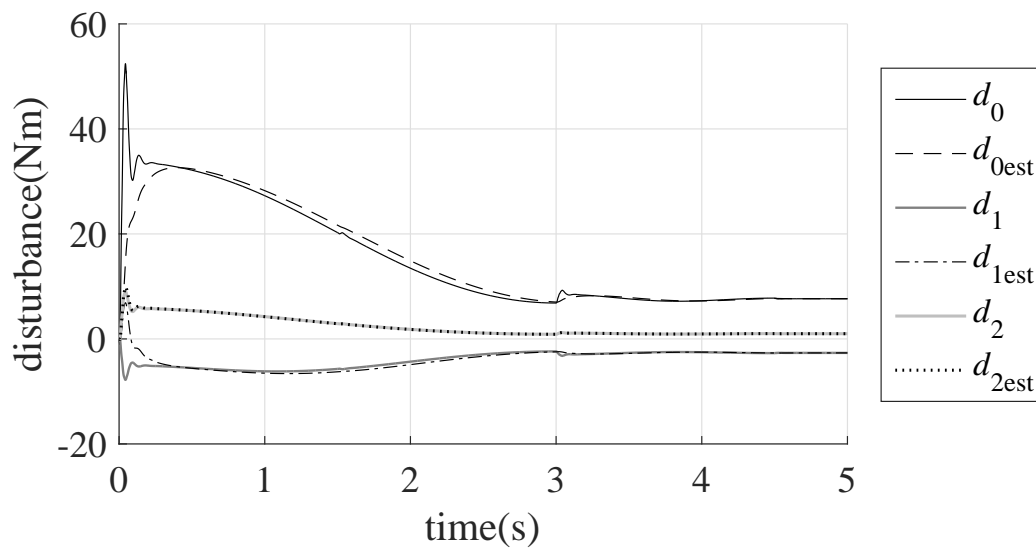


Fig. 5.8 Estimation result of disturbance

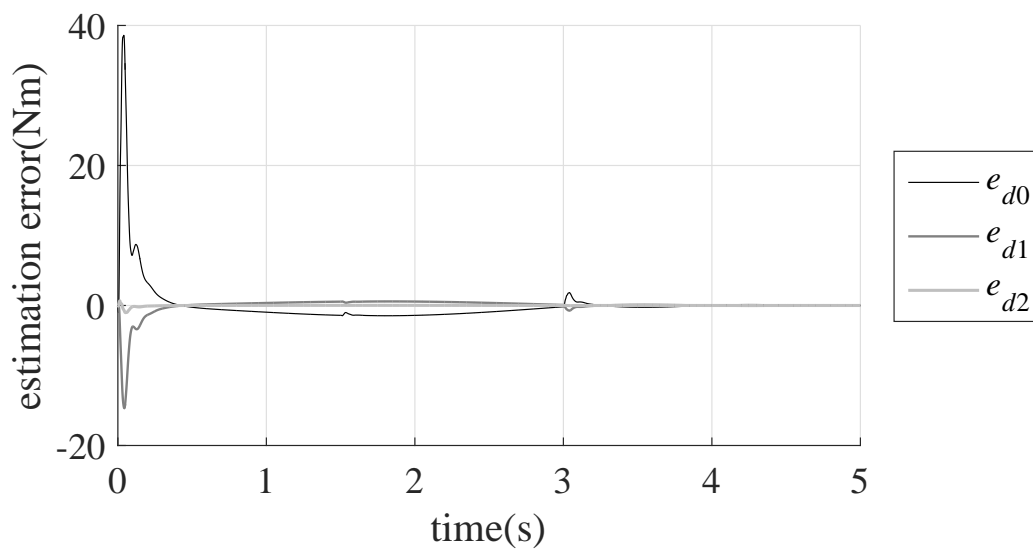


Fig. 5.9 Estimation error of disturbance

5.2 Disturbance Observer for Estimating Ground Reaction Force of a Quadruped Robot

5.2.1 Introduction

In this section, the disturbance observer proposed in section 5.1 is extended for estimation of ground reaction force. The 2-link 2-leg model is modified for more generality to be applied for various types of leg structure. In addition to the estimation of the support force provided by the hind legs, the ground reaction force acting on each leg is estimated by the extended observer. The performance of the extended observer is verified by simulations on the ODE.

5.2.2 Dynamics Model

To design a disturbance observer for estimation of ground reaction force, a simple dynamics model of a quadruped robot is derived. Generally complete dynamics of the quadruped robot is complex, therefore only the dynamics of the pitch motion in the sagittal plain is considered in this study by assuming that the motion around each axis can be decoupled. In the proposed model, the fore and hind legs are treated separately, and this brings a biped robot model which is supported by virtual reaction of the opposite legs. Figure 5.10 shows the model for the fore body. The hind legs are omitted in the proposed dynamics model but force acting on them including inertial force, gravitational force and ground reaction force is considered as the support force acting at the tip of the torso link. The model for the hind body can be derived in a similar manner. In the model, motion of links in a leg of a quadruped robot is described by a simple leg model with rotary motion of the hip joint and linear motion of the knee joint: The leg retraction/extension is approximated by linear motion, whereas the leg swing is performed by rotary motion typically in a quadruped robot. This approximation of the leg structure enables the disturbance observer to be applied to various quadruped robots because the two-dimensional geometry of the general robot's legs can be explained by the distance from a leg root to a leg tip and a leg angle, except for singular angles of rotary joints. By assuming that the magnitude of friction acting at the tip of the stance leg is sufficient, the slippage at the contact point can be neglected. This assumption brings the tip of the stance leg connected with the ground by a free hinge joint at the contact point. The notations are as follows: θ_{stance} , θ_{swing} ; relative angles of the hip joints, l_{stance} , l_{swing} ; distance between the COG of thigh and shin links,

θ_{tip} ; absolute angle of the shin link of the stance leg from the vertical axis, τ_{stance} , τ_{swing} ; input torque to the hip joints, f_{stance} , f_{swing} ; input force to the knee joints, l_{thigh} ; length of the hip joint axis to the COG of the thigh link, l_{shin} ; length from the tip of the leg to the COG of the shin link, l_{body} ; length from the hip joint axis to the COG of the torso link, $\mathbf{GRF}_{\text{stance}}$, $\mathbf{GRF}_{\text{swing}}$; ground reaction force at the leg tips of the stance and swing leg, and f_{hind} ; support force provided by the hind legs. In the proposed model, $\mathbf{GRF}_{\text{swing}}$ and f_{hind} are regarded as external disturbance force to the robot, where $\mathbf{GRF}_{\text{stance}}$ is included in the model implicitly because of the assumption that the robot is pinned at the contact point. The coordinate frame is based on the right-hand rule. The position and input vectors are defined as follows:

$$\boldsymbol{\theta} = [\theta_{\text{tip}} \quad l_{\text{stance}} \quad \theta_{\text{stance}} \quad \theta_{\text{swing}} \quad l_{\text{swing}}]^T \quad (5.20)$$

$$\boldsymbol{\tau} = [0 \quad f_{\text{stance}} \quad \tau_{\text{stance}} \quad \tau_{\text{swing}} \quad f_{\text{swing}}]^T \quad (5.21)$$

Consequently, the following equation of motion of the robot is obtained:

$$\mathbf{M}(\boldsymbol{\theta}) \ddot{\boldsymbol{\theta}} + \mathbf{r}(\boldsymbol{\theta}, \dot{\boldsymbol{\theta}}) + \mathbf{g}(\boldsymbol{\theta}) + \mathbf{c}(\dot{\boldsymbol{\theta}}) = \boldsymbol{\tau} + \sum \{ \mathbf{J}^T(\boldsymbol{\theta}) \mathbf{f} \} \quad (5.22)$$

where $\mathbf{M}(\boldsymbol{\theta})$ is an inertial matrix, $\mathbf{r}(\boldsymbol{\theta}, \dot{\boldsymbol{\theta}})$ is a nonlinear force/torque vector including centrifugal force, $\mathbf{g}(\boldsymbol{\theta})$ is a gravitational force/torque vector, $\mathbf{c}(\dot{\boldsymbol{\theta}})$ is a viscous resistance vector, \mathbf{f} is external disturbance force vectors and $\mathbf{J}(\boldsymbol{\theta})$ is Jacobian matrices corresponding to each external disturbance force vector.

5.2.3 Estimation of Ground Reaction Force

The disturbance observer for the estimation of ground reaction force is designed by the same manner as in section 5.1.3. The difference lies in the disturbance vector \mathbf{d} . In section 5.1.3, the disturbance vector does not include the effect of the ground reaction force. As the model proposed in this section includes the ground reaction force, the disturbance vector becomes as follows:

$$\mathbf{d} = \sum \{ \mathbf{J}^T(\mathbf{x}_1) \mathbf{f} \} = [d_0 \quad d_1 \quad d_2 \quad d_3 \quad d_4] \quad (5.23)$$

The external disturbance force $\mathbf{GRF}_{\text{swing}}$ and f_{hind} are distributed to each joint by the Jacobian matrices $\mathbf{J}_{\text{swing}}$ and \mathbf{J}_{hind} , respectively, whereas $\mathbf{GRF}_{\text{stance}}$ does not affect the motion of the robot in the proposed model. The distributed disturbance vectors are

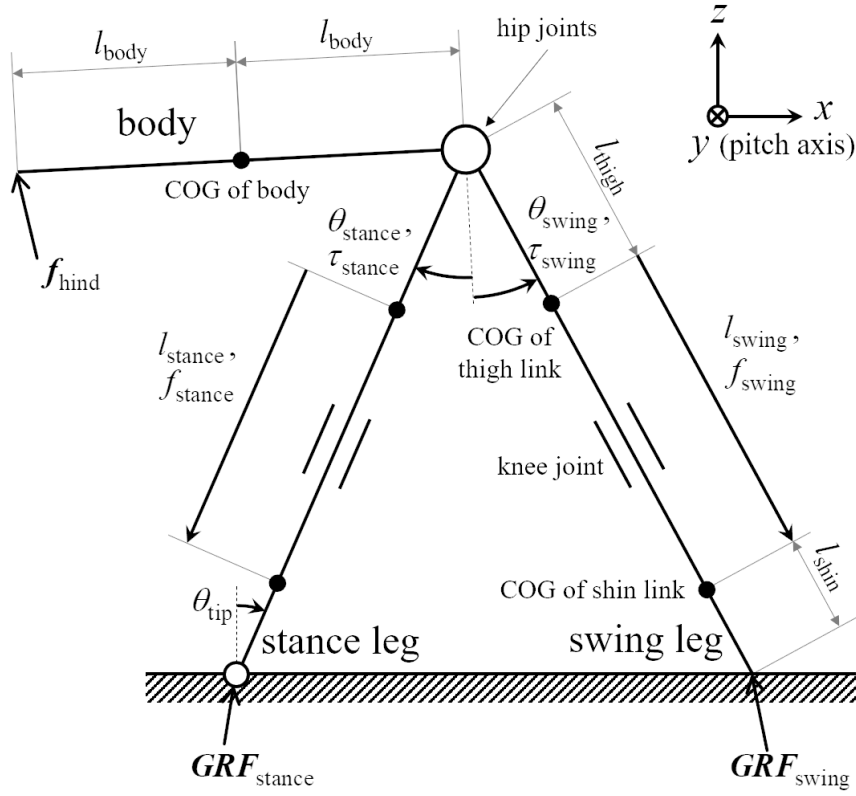


Fig. 5.10 Dynamics model for the observer design

defined as follows:

$$\mathbf{d}_{\text{swing}} = \mathbf{J}_{\text{swing}}^T \mathbf{GRF}_{\text{swing}} = \begin{bmatrix} d_{\text{swing}0} \\ d_{\text{swing}1} \\ d_{\text{swing}2} \\ d_{\text{swing}3} \\ d_{\text{swing}4} \end{bmatrix} \quad (5.24)$$

$$\mathbf{d}_{\text{hind}} = \mathbf{J}_{\text{hind}}^T \mathbf{f}_{\text{hind}} = \begin{bmatrix} d_{\text{hind}0} \\ d_{\text{hind}1} \\ d_{\text{hind}2} \\ 0 \\ 0 \end{bmatrix} \quad (5.25)$$

The 4th and 5th elements of \mathbf{d}_{hind} are zero because \mathbf{J}_{hind} does not contain θ_{swing} nor l_{swing} . The distributed vector is estimated by the observer without distinguishing source

of the disturbance, thus the disturbance vector is the summation of the disturbance vectors $\mathbf{d}_{\text{swing}}$ and \mathbf{d}_{hind} :

$$\mathbf{d} = \mathbf{d}_{\text{swing}} + \mathbf{d}_{\text{hind}} \quad (5.26)$$

As the 4th and 5th elements of \mathbf{d}_{hind} are zero, $\mathbf{GRF}_{\text{swing}}$ is estimated by the following equation:

$$\mathbf{GRF}_{\text{swing}}^{\hat{}} = \left(\mathbf{J}'_{\text{swing}} \right)^{-1} \begin{bmatrix} \hat{d}_3 \\ \hat{d}_4 \end{bmatrix}^{\text{T}} \quad (5.27)$$

where $\mathbf{J}'_{\text{swing}}$ is a square matrix composed of the 4th/5th rows and columns of $\mathbf{J}_{\text{swing}}$. \mathbf{f}_{hind} is estimated by subtracting the effect of $\mathbf{GRF}_{\text{swing}}^{\hat{}}$:

$$\hat{\mathbf{f}}_{\text{hind}} = \left(\mathbf{J}_{\text{hind}}^{\text{T}} \right)^+ \left(\hat{\mathbf{d}} - \mathbf{J}_{\text{swing}}^{\text{T}} \mathbf{GRF}_{\text{swing}}^{\hat{}} \right) \quad (5.28)$$

The notation \cdot^+ indicates the pseudo-inverse matrix. Summation of the external force including the gravitational force and the inertial force must be equal. However, the inertial force generally oscillates significantly, and estimation of the acceleration is difficult. Here it is assumed that the effect of acceleration is small enough; the torso of the robot moves forward with constant velocity and mass of all links is concentrated at the COG of the torso link because mass of the leg links is sufficiently small. Therefore $\mathbf{GRF}_{\text{stance}}$ is estimated by the following equation;

$$\mathbf{GRF}_{\text{stance}}^{\hat{}} = \begin{bmatrix} 0 \\ Mg \end{bmatrix} - \mathbf{GRF}_{\text{swing}}^{\hat{}} - \hat{\mathbf{f}}_{\text{hind}} \quad (5.29)$$

where M is the total mass of all links, g is the gravitational acceleration.

5.2.4 Simulation Conditions

Simulation of a quadruped robot utilizing the ODE was performed to examine the proposed disturbance observer. The robot model is shown in Fig. 5.11. Mass, moment of inertia and viscous coefficients of the robot model corresponding to the nominal model of the disturbance observer are shown in Table 5.3. The robot model has eight actuators in total, and two in each leg. The knee motion, i.e., leg retraction and extension, is performed by linear actuators attached to knee joints. The hip motion, i.e., leg swing in the pitch direction, is performed by rotary actuators attached to hip joints.

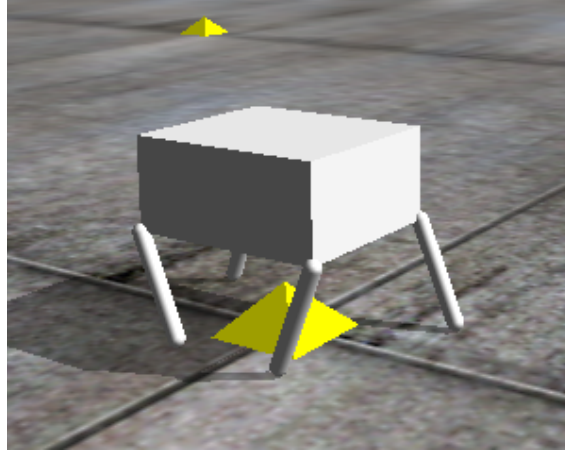


Fig. 5.11 Robot model for simulation

Table 5.3 Parameter values for the robot model

Parameter	Value	Parameter	Value
m_{shin}	1.00×10^{-2} kg	l_{shin}	1.75×10^{-2} m
m_{thigh}	1.00×10^{-2} kg	l_{thigh}	1.75×10^{-2} m
m_{torso}	1.00 kg	l_{torso}	6.00×10^{-2} m
I_{shin}	1.52×10^{-6} kgm ²	c_{hip}	1.00×10^{-2} kgm/s
I_{thigh}	1.52×10^{-6} kgm ²	c_{knee}	1.00 kg/s
I_{torso}	1.45×10^{-3} kgm ²		

It is assumed that the pitch angle of the robot's torso is measurable. In an actual robot, the measurement of the torso's pitch angle can be achieved by an attitude sensor of the body such as a gyroscope.

The robot motion is designed to achieve stable legged locomotion. In this simulation v , β and T in the equation of the locomotion parameters (Eq. (2.1)) are considered as independent parameters and s as a dependent parameter; therefore stride length s is calculated as follows:

$$s = v\beta T \quad (5.30)$$

Trajectories of leg joints during stance and swing phase are designed separately in leg

coordinate as shown in Fig. 5.12:

$$\theta(\phi) = \begin{cases} \theta_{\text{stance}}(\phi) & \text{for } 0 \leq \phi < \beta \\ \theta_{\text{swing}}(\phi) & \text{for } \beta \leq \phi < 1 \end{cases} \quad (5.31)$$

$$l(\phi) = \begin{cases} l_{\text{stance}}(\phi) & \text{for } 0 \leq \phi < \beta \\ l_{\text{swing}}(\phi) & \text{for } \beta \leq \phi < 1 \end{cases} \quad (5.32)$$

where $\phi = \frac{1}{T} \text{mod}(t, T)$ is a phase variable.

To avoid contact point slippage during the stance phase in each leg, the leg tip trajectory \mathbf{p} with constant velocity is designed as follows:

$$\mathbf{p}(\phi) = \begin{bmatrix} p_{x,\text{stance}}(\phi) \\ p_{z,\text{stance}}(\phi) \end{bmatrix} = \begin{bmatrix} s \left(\frac{\phi}{\beta} - \frac{1}{2} \right) \\ -z_{\text{stance}} \end{bmatrix} \quad \text{for } 0 \leq \phi < \beta \quad (5.33)$$

where z_{stance} is constant distance in z axis from the hip joint axis to the ground. Here, it is assumed that the torso link is horizontal to the ground. The joint trajectories of the stance leg θ_{stance} and l_{stance} are given by the following equation:

$$\begin{aligned} \theta_{\text{stance}}(\phi) &= \text{atan2} \{ p_{x,\text{stance}}(\phi), p_{z,\text{stance}}(\phi) \} \\ &= \text{atan2} \left\{ s \left(\frac{\phi}{\beta} - \frac{1}{2} \right), -z_{\text{stance}} \right\} \end{aligned} \quad (5.34)$$

$$l_{\text{stance}}(\phi) = \frac{z_{\text{stance}}}{\cos \{ \theta_{\text{stance}}(\phi) \}} - l_{\text{thigh}} - l_{\text{shin}} \quad (5.35)$$

The joint trajectories of the swing leg are designed so that the velocity of the joints is continuous at the phase transition. For the simplicity, the hip joint trajectory θ_{swing} is given by the polynomial equation:

$$\theta_{\text{swing}}(\phi) = \text{atan2} \left\{ \sum_{i=0}^3 a_i \left(\frac{\phi - \beta}{1 - \beta} \right)^i, -z_{\text{stance}} \right\} \quad (5.36)$$

The coefficient a_i is determined by the constraints such that the angle is smooth and the angular velocity is continuous at the phase transition. The knee joint trajectory l_{swing} is given by the following polynomial equation:

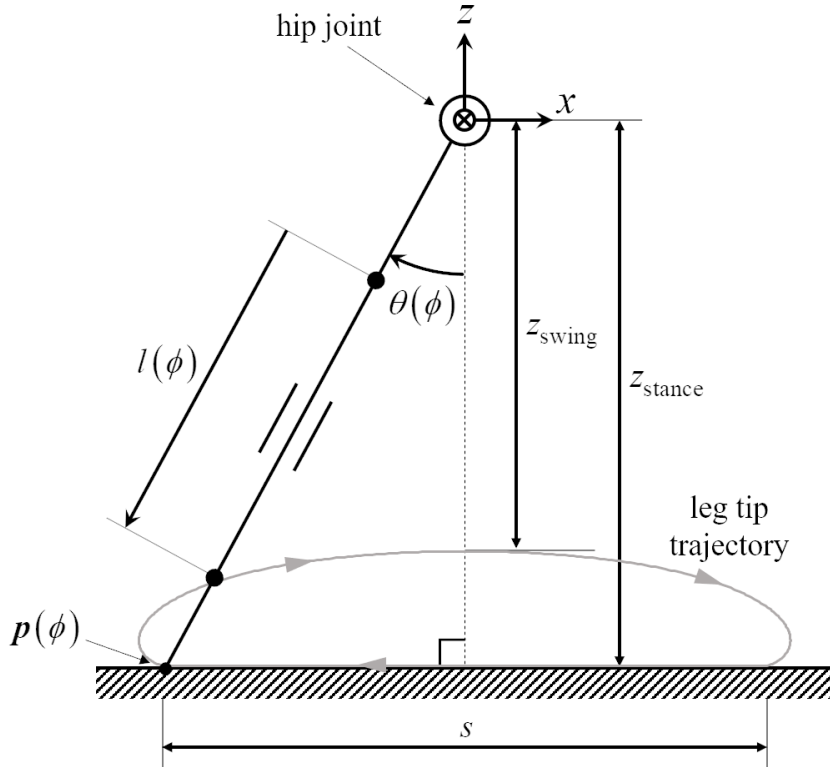


Fig. 5.12 Joint and leg tip trajectory in leg coordinate

$$l_{\text{swing}}(\phi) = \sum_{j=0}^4 b_j \left(\frac{\phi - \beta}{1 - \beta} \right)^j \quad (5.37)$$

where b_j is a coefficient of the polynomial equation. The constraints to determine b_j are as follows: Continuity in the velocity of l_{swing} is also desired at the phase transition. However, discontinuity is unavoidable because the leg tip velocity in z axis is minus at the end of stance phase, while the leg tip cannot move downward further to keep the torso link horizontal. Therefore, the velocity of l_{swing} at the phase transition is set to zero. The length is continuous at the phase transition. The leg tip reaches at the highest point z_{swing} at the middle of the swing phase. The resulting trajectories with respect to time t are shown in Fig. 5.13.

The parameters of the nominal model corresponds to ones of the simulation model. The observer gains shown in Table 5.4 were determined by trail and error.

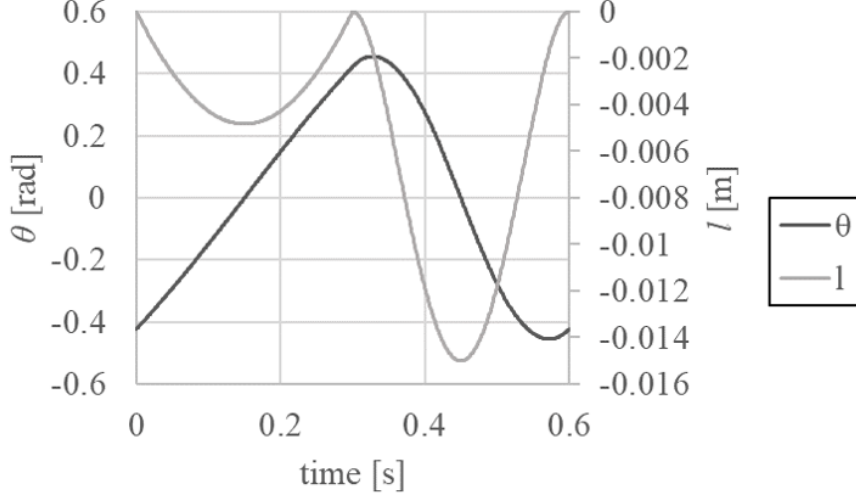


Fig. 5.13 Designed trajectories for leg joints. The parameters of the trajectories are as follows: $v = 0.15$ m/s, $\beta = 0.50$, $T = 0.60$ s, $s = 0.045$ m, $z_{\text{stance}} = 0.060$ m, $z_{\text{swing}} = 0.050$ m. The stance phase is from 0 s to 0.3 s and the swing phase is from 0.3 s to 0.6 s.

Table 5.4 Observer gains

Parameter	Value
$\alpha_{11} \cdots \alpha_{15}$	8.0
$\alpha_{21} \cdots \alpha_{25}$	0.30
$\alpha_{31} \cdots \alpha_{35}$	0.50
ε	1.0×10^{-4}

In each simulation, the robot walked for several locomotion periods so that the locomotion is stable. The initial values of the estimated states at $t = t_{\text{initial}}$ are set as the following equations:

$$\hat{\boldsymbol{x}}_{1,\text{initial}} = \hat{\boldsymbol{x}}_1(t_{\text{initial}}) = \boldsymbol{y}(t_{\text{initial}}) \quad (5.38)$$

$$\hat{\boldsymbol{x}}_{2,\text{initial}} = \hat{\boldsymbol{x}}_2(t_{\text{initial}}) = \mathbf{0} \quad (5.39)$$

$$\begin{aligned} \hat{\boldsymbol{d}}_{\text{initial}} &= \hat{\boldsymbol{d}}(t_{\text{initial}}) \\ &= \boldsymbol{J}_{\text{swing}}^{\text{T}}(\hat{\boldsymbol{x}}_{1,\text{initial}}) \begin{bmatrix} 0 \\ \frac{Mg}{2} \end{bmatrix} + \boldsymbol{J}_{\text{hind}}^{\text{T}}(\hat{\boldsymbol{x}}_{1,\text{initial}}) \begin{bmatrix} 0 \\ \frac{Mg}{2} \end{bmatrix} \end{aligned} \quad (5.40)$$

Here, it is assumed that the fore and hind legs support the robot's total mass equally. At the phase transition, the estimated disturbance $\hat{\boldsymbol{d}}$ is set to the initial value $\hat{\boldsymbol{d}}_{\text{initial}}$.

The simulation was performed for two trot locomotion conditions with different locomotion velocity because the trot locomotion is typical for higher speed motion control.

5.2.5 Simulation Results

The estimation results of the ground reaction force are shown in Figs. 5.14-5.17.

The ground reaction force acting on only right legs are shown because the ground reaction force acting on the right and left legs is almost symmetry. The notation above the figures show which of stance or swing phase models is applied for estimation.

The results show that the estimation of the ground reaction force is successful in the swing phase of each leg in all locomotion conditions even though the leg occasionally touches the ground because of inclination of the body. There is a slight difference in the estimation of the ground reaction force in the stance phase. This is because the ground reaction force of the stance leg is calculated with the support force provided by the opposite legs and its model includes modeling error such as ignoring roll motion of the torso, contact point slippage and inertial force. The error may accumulate largely on the estimation of the support force than the ground reaction force of the swing leg.

At the phase transition, the estimated ground reaction force shows an impulsive behavior as the estimated ground reaction force is set to the initial value.

5.2.6 Discussion

In this section, a disturbance observer design based on a high-gain observer structure for estimating ground reaction force of a quadruped robot was proposed. To design the disturbance observer, simple dynamics model of a general quadruped robot was derived. In the proposed dynamics model, the fore and hind legs are treated separately and external disturbance force including the ground reaction force and support force provided by opposite legs was estimated by the proposed disturbance observer. The disturbance observer could estimate the ground reaction force acting on the swing leg with sufficient accuracy. However, the ground reaction force of the stance leg was not estimated sufficiently because of the modeling error in a part of the dynamics regarding to the support force.

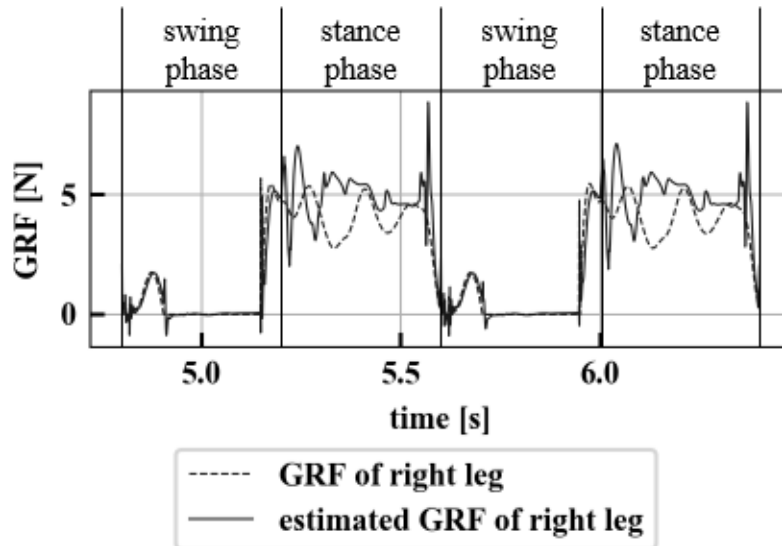


Fig. 5.14 Estimation results of ground reaction force on right legs. Locomotion conditions are as follows: $v = 0.10$ m/s, $\beta = 0.50$, $T = 0.80$ s, $s = 0.040$ m, fore.

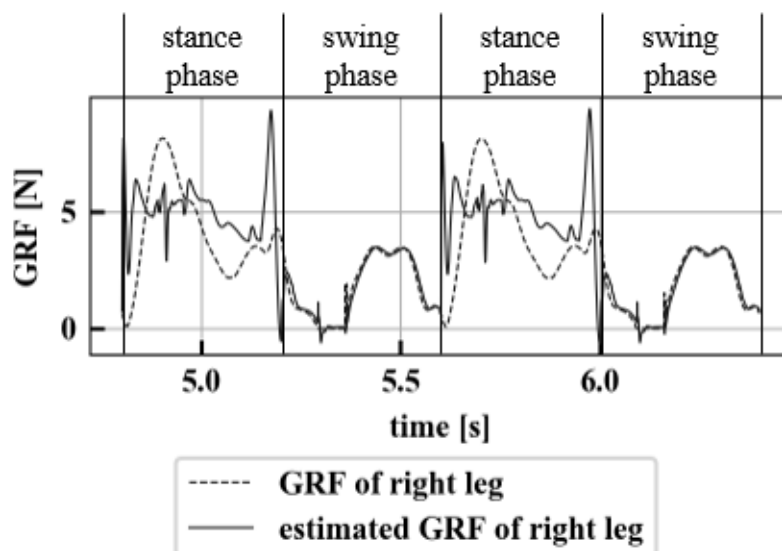


Fig. 5.15 Estimation results of ground reaction force on right legs. Locomotion conditions are as follows: $v = 0.10$ m/s, $\beta = 0.50$, $T = 0.80$ s, $s = 0.040$ m, hind.

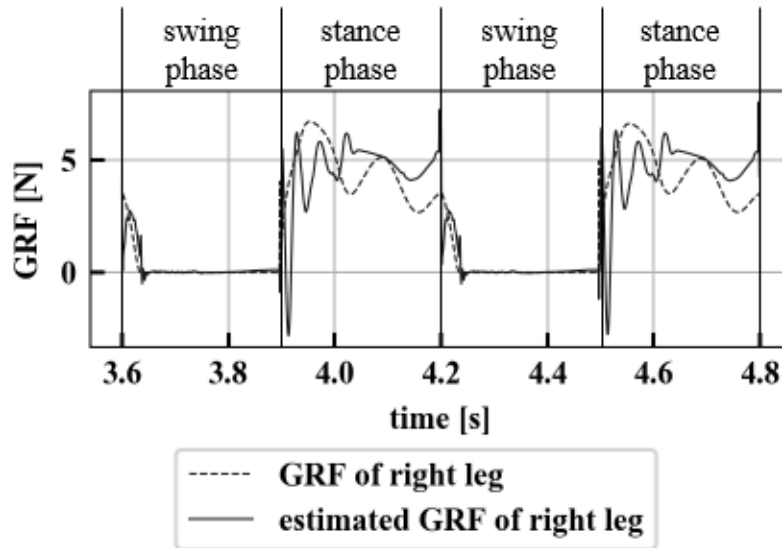


Fig. 5.16 Estimation results of ground reaction force on right legs. Locomotion conditions are as follows: $v = 0.15$ m/s, $\beta = 0.50$, $T = 0.60$ s, $s = 0.045$ m, fore.

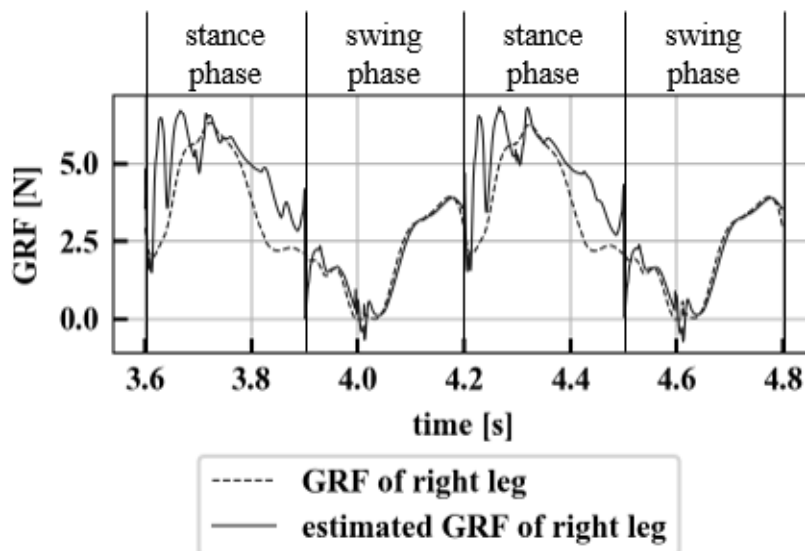


Fig. 5.17 Estimation results of ground reaction force on right legs. Locomotion conditions are as follows: $v = 0.15$ m/s, $\beta = 0.50$, $T = 0.60$ s, $s = 0.045$ m, hind.

Chapter 6

Conclusion

6.1 Summary

This study aimed to achieve the following two objectives for contributing to development of practical walking robots:

1. Propose a simple dynamics model for estimation of energy consumption for locomotion, which contributes to reducing the energy consumption of walking robots
2. Design a disturbance observer for estimation of ground reaction force, which can be applied to various controller designs such as CPG, ZMP and suppression of the energy consumption

To achieve those objectives, a novel 2-link 2-leg dynamics model for estimating energy consumption for locomotion is proposed and a disturbance observer utilizing the proposed model based on high-gain observer structure is designed for estimating disturbance and ground reaction force acting on walking robots. To examine the validity of the proposed 2-link 2-leg model and performance of the disturbance observer, the following works have been conducted:

- Validation of the energy consumption computed by utilizing the proposed model through experiments on an experimental quadruped robot
- Design of the basic structure of the disturbance observer for an experimental biped robot and its validation through simulations
- Extension of the disturbance observer for estimating the ground reaction force of a quadruped robot and its validation through simulations

Through those listed works, it is shown that the proposed model holds sufficient generality for estimating the energy consumption and applying to the nominal model of the disturbance observer despite approximation for reducing complexity of a walking robot. The performance of the disturbance observer based on the high-gain observer structure is also validated.

6.2 Discussion

In this section, problems which emerged in the experiments and simulations and possible solutions are discussed.

In the experiments of the energy consumption, the duty ratio hardly affected the robot's energy consumption. This might be because of the very low locomotion velocity and characteristics of the motors. The motors' output torque was high compared with the torque required to maintain the robot's posture. That leads less change in the energy consumption for different duty ratio because of the motors' high reduction ratio.

Further development of the experimental robot which has ability to perform locomotion with wider velocity range is required. The motors' output torque implemented in the experimental robot developed in this study cannot be measured, therefore other measurement method is required as well.

In this study, the qualitative comparison of the energy consumption profiles obtained from the proposed model and the experimental robot is discussed. However, it is required to consider the quantitative comparison for the precise estimation.

Future work will include mathematical analysis of energy consumption utilizing equations of the proposed model as the proposed model is sufficiently simple to derive effects of the locomotion parameters mathematically. To apply the proposed model to an actual robot and obtain precise estimation of the energy consumption, approximation of actual robot's leg structure to the proposed dynamics model must be considered.

In the simulations of the disturbance observer for the quadruped robot, the ground reaction force of the stance leg was not estimated sufficiently. This is because of the modeling error in a part of the dynamics regarding to the support force. The assumption that the torso acceleration is negligible might not be appropriate.

Floating base model is one of the candidates of improved dynamics model because the accumulation of the error and impulsive outputs at the phase transition can be avoided. Application of the disturbance observer to an actual quadruped robot is necessary as well. To achieve the application, it is also essential to design a method for approximating leg structure of the actual robot to the proposed dynamics model.

In the last of the thesis, the future prospectives of the achievement are discussed. As the disturbance observer has sufficient performance to estimate the disturbance and ground reaction force, it is expected to apply it to controller designs requiring measurement of the ground reaction force such as CPG modulated by the ground reaction force.

In combination of the proposed model and disturbance observer, it is also expected unraveling the mechanism of the energy-optimal gait transitions by considering the ground reaction force and achieving the energy-optimal locomotion utilizing sensor-less detection of the ground reaction force is achieved in the future.

Bibliography

- [1] Tokyo Electric Power Company Holdings, Inc., “福島第一原子力発電所 3 号機タービン建屋における協力企業作業員の被ばくに関する調査結果について”, http://www.tepco.co.jp/nu/f1-np/press_f1/2010/htmldata/bi1386-j.pdf, 25th March, 2011, accessed on 16th February, 2019. (in Japanese)
- [2] Ministry of Health, Labour and Welfare, Japan, “介護保険事業状況報告”, 2015. (in Japanese)
- [3] THE SANKEI NEWS, “建設現場に四足歩行ロボット 竹中とフジタが実証実験”, <https://www.sankei.com/economy/news/180625/ecn1806250023-n1.html>, 25th June, 2018, accessed on 16th February, 2019. (in Japanese)
- [4] Ministry of Finance, Japan, “財務省広報誌「ファイナンス」”, https://www.mof.go.jp/public_relations/finance/201810/201810l.pdf, October, 2018, accessed on 16th February, 2019. (in Japanese)
- [5] S. Tadokoro, “Present Situation and Future Prospects of Rescue Robots”, The journal of the Institute of Electronics, Information and Communication Engineers, Vol.92, No.3, pp.203-208, 2009. (in Japanese)
- [6] FANUC, “PAINTING ROBOTS”, <https://www.fanucamerica.com/industrial-solutions/manufacturing-applications/painting-robots>, accessed on 16th February, 2019.
- [7] S. Tadokoro, “Middle-Long Term Issues of Disaster Robots in Japan”, Journal of the Robotics Society of Japan, Vol.32, No.2, pp.154-161, DOI:10.7210/jrsj.32.154, 2014. (in Japanese)
- [8] Nikkan Kogyo Shimbun (The Daily Industrial News), “厚労省、介護ロボット協議会立ち上げへ 主役は「現場」、問題抽出・開発に反映”, <https://www.nikkan.co.jp/articles/view/00371410>, 19th January, 2016, accessed on 16th February, 2019. (in Japanese)
- [9] SONY, “aibo”, <https://us.aibo.com/>, accessed on 16th February, 2019.
- [10] Honda Motor Co., Ltd., “Honda Robotics”,

- <https://global.honda/innovation/robotics.html>, accessed on 16th February, 2019.
- [11] Boston Dynamics, “SpotMini”, <https://www.bostondynamics.com/spot-mini>, accessed on 16th February, 2019.
- [12] Takenaka Corporation, “竹中工務店、ソフトバンクロボティクス、ソフトバンクの3社で建設現場における Boston Dynamics 社の「SpotMini」の活用に向けた実証実験を実施”, <http://www.takenaka.co.jp/news/2018/06/01/index.html>, 25th June, 2018, accessed on 16th February, 2019. (in Japanese)
- [13] The Guardian, “SpotMini: headless robotic dog to go on sale in 2019”, <https://www.theguardian.com/technology/2018/may/14/spotmini-robotic-dog-sale-2019-former-google-boston-dynamics>, 14th May, 2018, accessed on 16th February, 2019.
- [14] S. Kajita, F. Kanehiro, K. Kaneko, K. Fujiwara, K. Harada, K. Yokoi and H. Hirukawa, “Biped Walking Pattern Generation by using Preview Control of Zero-Moment Point”, Proceedings of the 2003 IEEE International Conference on Robotics & Automation, pp.1620-1626, DOI:10.1109/ROBOT.2003.1241826, Taipei, Taiwan, September, 2003.
- [15] M. Vukobratovic and J. Stepanenko, “On the stability of anthropomorphic systems”, *Mathematical Biosciences*, Vol.15, No.1, pp.1-37, DOI:10.1016/0025-5564(72)90061-2, October, 1972.
- [16] S. Zhang, J. Gao, X. Duan, H. Li, Z. Yu, X. Chen, J. Li, H. Liu, X. Li, Y. Liu and Z. Xu, “Trot Pattern Generation for Quadruped Robot Based on the ZMP Stability Margin”, Proceedings of 2013 ICME International Conference on Complex Medical Engineering, pp.608-613, DOI:10.1109/ICCME.2013.6548322, Beijing, China, May, 2013.
- [17] R. Kurazume, K. Yoneda and S. Hirose, “3D Sway Compensation Trajectory for Quadruped Walking Robot”, *Journal of the Robotics Society of Japan*, Vol.19, No.5, pp.632-637, DOI:10.7210/jrsj.19.632, 2001. (in Japanese)
- [18] H. Osumi, S. Kamiya, H. Kato, K. Umeda, R. Ueda and T. Arai, “Time Optimal Control for Quadruped Walking Robots”, Proceedings of the 2006 IEEE International Conference on Robotics and Automation, pp.1102-1108, DOI:10.1109/ROBOT.2006.1641857, Orlando, USA, May, 2006.
- [19] Y. Suzuki and H. Osumi, “Time optimal positioning control of a quadruped robot for trot gait”, *Transactions of the Japan Society of Mechanical Engineers*, Vol.83, No.849, pp.17-00017, DOI:10.1299/transjsme.17-00017, 2017. (in Japanese)

-
- [20] R. Kurazume, K. Yoneda and S. Hirose, "Feedforward and feedback dynamic trot gait control for a quadruped walking vehicle", *Autonomous Robotics*, Vol.12, No.2, pp.157-172, DOI:10.1023/A:1014045326702, 2002.
- [21] N. Motoi, K. Sasahara, and A. Kawamura, "Switching Control Method for Stable Landing by Legged Robot Based on Zero Moment Point", *Journal of Robotics and Mechatronics*, Vol.25, No.5, pp.831-839, DOI:10.20965/jrm.2013.p0831, 2013.
- [22] P. R. Vundavilli and D. K. Pratihari, "Dynamically balanced optimal gaits of a ditch-crossing biped robot", *Robotics and Autonomous Systems*, Vol.58, No.4, pp.349-361, DOI:10.1016/j.robot.2009.10.004, 2010.
- [23] S. Kitano, S. Hirose, A. Horigome and G. Endo, "TITAN-XIII sprawling-type quadruped robot with ability of fast and energy-efficient walking", *ROBOMECH Journal*, Vol.3, No.8, DOI:10.1186/s40648-016-0047-1, 2016.
- [24] R. Horio, N. Uchiyama and S. Sano, "Trot Gait Control of Quadruped Robot Based on Inclination of Body", *Proceedings of the 2014 IEEE International Conference on Robotics and Biomimetics*, pp.2026-2067, DOI:10.1109/ROBIO.2014.7090640, Bali, Indonesia, December, 2014.
- [25] M. Focchi, A. D. Prete, I. Havoutis, R. Featherstone, D. G. Caldwell and C. Semini, "High-slope Terrain Locomotion for Torque-Controlled Quadruped Robots", *Autonomous Robotics*, Vol.41, No.1, pp.259-272, DOI:10.1007/s10514-016-9573-1, 2017.
- [26] G. Zhang, X. Rong, C. Hui, Y. Li and B. Li, "Torso motion control and toe trajectory generation of a trotting quadruped robot based on virtual model control", *Advanced Robotics*, Vol.30, No.4, pp.284-297, DOI:10.1080/01691864.2015.1113889, 2015.
- [27] S. Alfayad, O. Bruneau, F. B. Ouezdou, M. A. Fouz, P. F. Douliez, "Analytical Energetic Approach for Predictive Generation of Dynamic Biped Walking - Use of Average Energies", *International Review of Mechanical Engineering*, Vol.10, No.7, pp.461-473, DOI:10.15866/ireme.v10i7.8863, 2016.
- [28] X. Li, H. Imanishi, M. Minami, T. Matsuno, and A. Yanou, "Dynamical Model of Walking Transition Considering Nonlinear Friction with Floor", *Journal of Advanced Computational Intelligence and Intelligent Informatics*, Vol.20, No.6, pp.974-982, DOI:10.20965/jaciii.2016.p0974, 2016.
- [29] A. Syuhri, H. A. Basuki and S. N. H. Syuhri, "Kinematics Analysis of a Leg Mechanism as a Motion Converter", *International Review of Mechanical Engineering*, Vol.10, No.6, pp.409-418, DOI:10.15866/ireme.v10i6.10011, 2016.

- [30] A. Rosendo, S. Nakatsu, X. Liu, M. Shimizu and K. Hosoda, “Quadrupedal locomotion based on a muscular activation pattern with stretch-reflex”, Proceedings of the 2014 IEEE International Conference on Robotics and Biomimetics, pp.773-778, DOI:10.1109/ROBIO.2014.7090425, Bali, Indonesia, December, 2014.
- [31] S. Nakatsu, A. Rosendo, M. Shimizu and K. Hosoda, “Realization of Three-dimensional Walking of a Cheetah-modeled Bio-inspired Quadruped Robot”, Proceedings of the 2014 IEEE International Conference on Robotics and Biomimetics, pp.779-784, DOI:10.1109/ROBIO.2014.7090426, Bali, Indonesia, December, 2014.
- [32] M. Mutlu, S. Hauser, A. Bernardino and A. J. Ijspeert, “Effects of passive and active joint compliance in quadrupedal locomotion”, *Advanced Robotics*, Vol.32, No.15, pp.809-824, DOI:10.1080/01691864.2018.1497535, 2018.
- [33] S. Hauser, M. Mutlu, P. Banzet and A. J. Ijspeert, “Compliant universal grippers as adaptive feet in legged robots”, *Advanced Robotics*, Vol.32, No.15, pp.825-836, DOI:10.1080/01691864.2018.1496851, 2018.
- [34] S. Zhigailov, V. Musalimov, G. Aryassov and I. Penkov, “Modelling and Simulation of Human Lower-Limb Motion”, *International Review on Modelling and Simulations*, Vol.9, No.2, pp.114-123, DOI:10.15866/iremos.v9i2.8358, 2016.
- [35] M. R. Hirt, W. Jetz, B. C. Rall and U. Brose, “A general scaling law reveals why the largest animals are not the fastest”, *Nature Ecology & Evolution*, Vol.1, pp.1116-1122, DOI:10.1038/s41559-017-0241-4, August, 2017.
- [36] J. Ackerman and J. Seipel, “Energetics of bio-inspired legged robot locomotion with elastically-suspended loads”, Proceedings of the 2011 IEEE/RSJ International Conference on Intelligent Robots and Systems, pp.203-208, DOI:10.1109/IROS.2011.6095153, San Francisco, USA, September, 2011.
- [37] V. A. Tucker, “The Energetic Cost of Moving About: Walking and running are extremely inefficient forms of locomotion. Much greater efficiency is achieved by birds, fish and bicyclists”, *American Scientist*, Vol.63, No.4, pp.413-419, 1975.
- [38] C. Caceres, J. Puerta, R. Jiménez, D. Rojas, “Design of a Bio-Inspired Equine Robot Prototype”, *International Review of Mechanical Engineering*, Vol.10, No.1, pp.12-17, DOI:10.15866/ireme.v10i1.7672, 2016.
- [39] L. Minati, M. Frasca, N. Yoshimura and Y. Koike, “Versatile Locomotion Control of a Hexapod Robot Using Hierarchical Network of Nonlinear Oscillator Circuits”, *IEEE Access*, Vol.6, pp.8042-8065, DOI:10.1109/ACCESS.2018.2799145, 2018.
- [40] A. Fukuhara, D. Owaki, T. Kano, R. Kobayashi and A. Ishiguro, “Sponta-

- neous gait transition to high-speed galloping by reconciliation between body support and propulsion”, *Advanced Robotics*, Vol.32, No.15, pp.794-808, DOI:10.1080/01691864.2018.1501277, 2018.
- [41] D. Owaki and A. Ishiguro, “A Quadruped Robot Exhibiting Spontaneous Gait Transitions from Walking to Trotting to Galloping”, *Scientific Reports*, Vol.7, DOI:10.1038/s41598-017-00348-9, 2017.
- [42] Y. Fukuoka and H. Kimura, “Realization of Dynamic Turning Motion of Irregular Terrain of a Quadruped Robot “TEKKEN4” with Neural Oscillators”, *Transactions of the Japan Society of Mechanical Engineers C*, Vol.72, No.724, pp.3848-3854, DOI:10.1299/kikaic.72.3848, 2006. (in Japanese)
- [43] Y. Fukuoka, Y. Habu and T. Fukui, “A simple rule for quadrupedal gait generation determined by leg loading feedback: a modeling study”, *Scientific Reports*, Vol.5, DOI:10.1038/srep08169, 2015.
- [44] Y. Fukuoka and H. Kimura, “A Quadruped Robot Walking and Running with One Mechanism”, *Transactions of the Japan Society of Mechanical Engineers C*, Vol.75, No.750, DOI:10.1299/kikaic.75.390, 2009. (in Japanese)
- [45] A. Spöwitz, A. Tuleu, M. Vespignani, M. Ajallooeian, E. Badri and A. J. Ijspeert, “Towards dynamic trot gait locomotion: Design, control, and experiments with Cheetah-cub, a compliant quadruped robot”, *The International Journal of Robotics Research*, Vol.32, No.8, pp.932-950, DOI:10.1177/0278364913489205, 2013.
- [46] A. M. Kassim, T. Yasuno, N. Abas, M. S. M. Aras and M. Z. A. Rashid, “Performance Study of Reference Height Control Algorithm for Tripod Hopping Robot”, *International Review of Mechanical Engineering*, Vol.7, No.5, pp.784-789, 2013.
- [47] M. Ajallooeian, S. Gay, A. Tuleu, A. Spöwitz and A. J. Ijspeert, “Modular Control of Limit Cycle Locomotion over Unperceived Rough Terrain”, *Proceedings of the 2013 IEEE/RSJ International Conference on Intelligent Robots and Systems*, pp.3390-3397, DOI:10.1109/IROS.2013.6696839, Tokyo, Japan, November, 2013.
- [48] A. J. Ijspeert, “Central pattern generators for locomotion control in animals and robots: A review”, *Neural Networks*, Vol.21, pp.642-653, DOI:10.1016/j.neunet.2008.03.014, 2008.
- [49] K. Tsujita, K. Tsuchiya and A. Onat, “Adaptive gait pattern control of a quadruped locomotion robot”, *Proceedings of 2001 IEEE/RSJ International Conference on Intelligent Robots and Systems*, pp.2318-2325, DOI:10.1109/IROS.2001.976416, Maui, USA, October, 2001.

- [50] K. Matsuoka, "Sustained Oscillations Generated by Mutually Inhibiting Neurons with Adaptation", *Biological Cybernetics*, Vol.52, No.6, pp.367-376, DOI:10.1007/BF00449593, 1985.
- [51] A. Ananthanarayanan, M. Azadi and S. Kim, "Towards a bio-inspired leg design for high-speed running", *Bioinspiration & Biomimetics*, Vol.7, No.4, DOI:10.1088/1748-3182/7/4/046005, 2012.
- [52] S. Seok, A. Wang, M. Y. (M.) Chuah, D. Otten, J. Lang and S. Kim, "Design Principles for Highly Efficient Quadrupeds and Implementation on the MIT Cheetah Robot", *Proceedings of the 2013 IEEE International Conference on Robotics and Automation*, pp.3292-3297, DOI:10.1109/ICRA.2013.6631038, Karlsruhe, Germany, May, 2013.
- [53] S. Seok, A. Wang, D. Otten and S. Kim, "Actuator Design for High Force Proprioceptive Control in Fast Legged Locomotion", *Proceedings of the 2012 IEEE/RSJ International Conference Intelligent Robots and Systems*, pp.1970-1975, DOI:10.1109/IROS.2012.6386252, Vilamoura, Portugal, October, 2012.
- [54] P. M. Krishna and R. P. Kumar, "Energetics of Constant Height Level Bounding in Quadruped Robots", *Robotica*, Vol.34, No.2, pp.403-422, DOI:10.1017/S0263574714001532, 2016.
- [55] H. Gao, Y. Liu, L. Ding, G. Liu, Z. Deng, Y. Liu and H. Yu, "Low Impact Force and Energy Consumption Motion Planning for Hexapod Robot with Passive Compliant Ankles", *Journal of Intelligent & Robotic Systems*, DOI:10.1007/s10846-018-0828-2, 2018.
- [56] D. F. Hoyt and C. R. Taylor, "Gait and the energetics of locomotion in horses", *Nature*, Vol.292, pp.239-240, DOI:10.1038/292239a0, 1981.
- [57] T. M. Griffin, R. Kram, S. J. Wickler and D. F. Hoyt, "Biomechanical and energetic determinants of the walk-trot transition in horses", *The Journal of Experimental Biology*, Vol.207, pp.4215-4223, DOI:10.1242/jeb.01277, 2004.
- [58] T. M. Griffin, R. P. Main and C. T. Farley, "Biomechanics of quadrupedal walking: how do four-legged animals achieve inverted pendulum-like movements?", *The Journal of Experimental Biology*, Vol.207, pp.3545-3558, DOI:10.1242/jeb.01177, 2004.
- [59] A. Y. Vukolov, O. V. Egorova, "Research on Biological Locomotion with Usage of Modern Digital Strobelight Photographic Technique", *International Review of Mechanical Engineering*, Vol.11, No.5, pp.286-293, DOI:10.15866/ireme.v11i5.11610,

- 2017.
- [60] J. Nishii, “An analytical estimation of the energy cost for legged locomotion”, *Journal of Theoretical Biology*, Vol.238, pp.636-645, DOI:10.1016/j.jtbi.2005.06.027, 2006.
- [61] J. Nishii, “Legged insects select the optimal locomotor pattern based on the energetic cost”, *Biological Cybernetics*, Vol.83, No.5, pp.435-442, DOI:10.1007/s004220000175, 2000.
- [62] Y. Fukuoka, K. Fukino, Y. Habu and Y. Mori, “Energy evaluation of a bio-inspired gait modulation method for quadrupedal locomotion”, *Bioinspiration & Biomimetics*, Vol.10, No.4, DOI:10.1088/1748-3190/10/4/046017, 2015.
- [63] K. Kiguchi, Y. Kusumoto, K. Watanabe, K. Izumi and T. Fukuda, “Energy-optimal gait analysis of quadruped robots”, *Artificial Life and Robotics*, Vol.6, No.3, pp.120-125, DOI:10.1007/BF02481325, 2002.
- [64] M. Camurri, M. Fallon, S. Bazeille, A. Radulescu, V. Barasuol, D. G. Caldwell and C. Semini, “Probabilistic Contact Estimation and Impact Detection for State Estimation of Quadruped Robots”, *IEEE Robotics and Automation Letters*, Vol.2, No.2, pp.1023-1030, DOI:10.1109/LRA.2017.2652491, 2017.
- [65] R. Smith, “Open Dynamics Engine v0.5 User Guide”, <http://ode.org/ode-latest-userguide.html>, accessed on 16th February, 2019.
- [66] The Japan Society of Mechanical Engineers, “Robotics”, pp.41-52, The Japan Society of Mechanical Engineers, 2011. (in Japanese)
- [67] R. Horio, N. Uchiyama and S. Sano, “Observer Design for Estimating Support Force Applied by a Human Operator of a Biped Robot”, *Journal of Advanced Computational Intelligence and Intelligent Informatics*, Vol.21, No.4, pp.744-750, DOI:10.20965/jaciii.2017.p0744, 2017.
- [68] Honda Motor Co., Ltd., “力丸 HP350”, <http://www.honda.co.jp/carrier/products/hp350.html>, accessed on 16th February, 2019. (in Japanese)
- [69] A. Sano, S. Tamegai, K. Iwatsuki, N. Ota, Y. Ikemata and H. Fujimoto, “Development of Multi-role Bipedal Walker Based on Human-assisted Passive Walking (1) : Legged Transport, Walk-assist, and WalkerTrial”, *The Proceedings of JSME annual Conference on Robotics and Mechatronics*, pp.1A2-A12(2), DOI:10.1299/jsmermd.2010._1A2-A12_1, Asahikawa, Japan, June, 2010. (in Japanese)
- [70] S. Nakajima and E. Nakano, “Adaptive Gait for Large Rough Terrain of a

- Leg-wheel Robot : 2nd Report, Gait for an Upward Step”, Transactions of the Japan Society of Mechanical Engineers C, Vol.72, No.721, pp.2932-2939, DOI:10.1299/kikaic.72.2926, 2006. (in Japanese)
- [71] K. Hashimoto, Y. Sugahara, H. Lim and A. Takanishi, “New Biped Foot System Adaptable to Uneven Terrain”, *Journal of Robotics and Mechatronics*, Vol.18, No.3, pp.271-277, DOI:10.20965/jrm.2006.p0271, 2006.
- [72] K. Hashimoto, Y. Sugahara, M. Kawase, A. Hayashi, C. Tanaka and A. Ohta, “Realization of Outdoor Human-carrying Biped Walking by Landing Pattern Modification Method”, *The Robotics Society of Japan*, Vol.25, No.6, pp.851-859, DOI:10.7210/jrsj.25.851, 2007. (in Japanese)
- [73] T. Takuma and K. Hosoda, “Terrain Negotiation of a Compliant Biped Robot Driven by Antagonistic Artificial Muscles”, *Journal of Robotics and Mechatronics*, Vol.19, No.4, pp.423-428, DOI:10.20965/jrm.2007.p0423, 2007.
- [74] K. Harada, M. Morisawa, S. Nakaoka, K. Kaneko and S. Kajita, “Kinodynamic Planning for Humanoid Robots Walking on Uneven Terrain”, *Journal of Robotics and Mechatronics*, Vol.21, No.3, pp.311-316, DOI:10.20965/jrm.2009.p0311, 2009.
- [75] E. Ohashi, T. Sato and K. Ohnishi, “A Walking Stabilization Method Based on Environmental Modes on Each Foot for Biped Robot”, *IEEE Transactions on Industrial Electronics*, Vol.56, No.10, pp.3964-3974, DOI:10.1109/TIE.2009.2024098, 2009.
- [76] K. Hyodo, S. Mikami and S. Suzuki, “Outdoor Environments Walking by Biped Passive Dynamic Walker with Constraint Mechanism”, *Journal of Robotics and Mechatronics*, Vol.22, No.3, pp.363-370, DOI:10.20965/jrm.2010.p0363, 2010.
- [77] K. Hyodo, T. Oshimura, S. Mikami and S. Suzuki, “Stabilizing Passive Dynamic Walk Under Wide Range of Environments by Constraint Mechanism Fitted to Sole of Foot”, *Journal of Robotics and Mechatronics*, Vol.21, No.3, pp.403-411, DOI:10.20965/jrm.2009.p0403, 2009.
- [78] T. Yokomichi and N. Ushimi, “A Study of the Sole Mechanism of Biped Robots to Rough Terrain Locomotion”, *Journal of Robotics and Mechatronics*, Vol.24, No.5, pp.902-907, DOI:10.20965/jrm.2012.p0902, 2012.
- [79] T. Aoyama, K. Sekiyama, Y. Hasegawa and T. Fukuda, “PDAC-Based 3-D Biped Walking Adapted to Rough Terrain Environment”, *Journal of Robotics and Mechatronics*, Vol.24, No.1, pp.37-46, DOI:10.20965/jrm.2012.p0037, 2012.
- [80] M. Yamada, H. Maie, Y. Maeno, S. Sano and N. Uchiyama, “Design of point-contact type foot with springs for biped robot”, *Proceedings of the 2010 IEEE/ASME*

-
- International Conference on Advanced Intelligent Mechatronics, pp.806-811, DOI:10.1109/AIM.2010.5695760, Montreal, Canada, July, 2010.
- [81] S. Sano, M. Yamada, N. Uchiyama and S. Takagi, “Point-contact type foot with springs and posture control for biped walking on rough terrain”, Proceedings of the 2008 10th IEEE International Workshop on Advanced Motion Control, pp.480-485, DOI:10.1109/AMC.2008.4516114, Trento, Italy, March, 2008.
- [82] M. -S. Kim, J. -H. Kim, M. -G. Choi and J. -W. Kim, “A New Trajectory Generation Scheme for Direction Turning in Biped Walking”, Journal of Advanced Computational Intelligence and Intelligent Informatics, Vol.14, No.5, pp.550-554, DOI:10.20965/jaciii.2010.p0550, 2010.
- [83] N. Uchiyama, D. Kurita and S. Sano, “Design and control of a human-operated biped robot for transportation of objects”, Journal of Robotics and Mechatronics, Vol.26, No.6, pp.750-757, DOI:10.20965/jrm.2014.p0750, 2014.
- [84] H. K. Khalil, “Nonlinear Systems Third Edition”, Prentice Hall, Inc., 2002.

Acknowledgment

本研究を行うにあたり，多大なご指導を賜りました豊橋技術科学大学機械工学系 内山直樹教授に心よりお礼申し上げます。提出期限を破ってばかりの私でしたが，辛抱強く，手厚くご指導してくださり，誠にありがとうございます。

博士前期・後期課程在学中におきましては，豊橋技術科学大学リーディング大学院プログラムおよびテラーメイド・バトンゾーン教育プログラムより研究活動に関して，また経済的な面に関して様々なご支援を賜りました。貴学のご支援により本研究の機会を得られましたことに感謝申し上げます。リーディング大学院プログラムにて指導教員としてご指導くださりました，University of Stuttgart, Institute for System Dynamics, Oliver Sawodny 教授，社会福祉法人 名古屋市総合リハビリテーション事業団 鈴木光久様にお礼申し上げます。また，博士後期課程実務訓練でお世話になりました，NTT データ経営研究所の皆様にも厚くお礼申し上げます。

私の至らなさのためにリーディング大学院プログラムを修了することは叶いませんでしたが，履修課程で得られた知識・経験は今後も私を助け導いてくれるものであると確信しております。

研究を共にし，白熱した議論を繰り広げたシステム工学研究室，ロボティクス・メカトロニクス研究室のみんなのおかげで，非常に充実した学生生活を送ることができました。みんな抜きではさぞや味気のない学生生活を送っていたことでしょう。

最後に，これまで長きにわたる学生生活を暖かく見守ってくれた両親にこの場を借りてお礼申し上げます。

手短ではありますが，以上を感謝の言葉とさせていただきます。本当にありがとうございました。